Characterization of echoes:
toy models and compact objects

Miguel Alexandre Ribeiro Correia

Thesis to obtain the Master of Science Degree in

Engineering Physics

Supervisor: Prof. Dr. Vítor Cardoso

Examination Committee

Chairperson: Prof. Dr. José Lemos

Supervisor: Prof. Dr. Vítor Cardoso

Member of the Committee: Prof. Dr. José Natário

June 2018

Acknowledgments

I would like to manifest my sincere thanks to the following:

First and foremost, to my supervisor Professor Vítor Cardoso for presenting me a challenging problem and supporting me throughout the preparation of this dissertation and more than a year of research that culminated in a jointly authored publication of the work presented herein. But in particular, for his genuine interest in my ideas and his considerate and thoughtful way of answering all my doubts and difficult questions.

To the Multidisciplinary Center for Astrophysics (CENTRA) and its theoretical division Gravitation in Técnico (GRIT) whose weekly meetings I had the pleasure to co-preside in the past year. The CENTRA seminars and the dynamical discussions with GRIT members were of great value for both my personal and technical growths as a young researcher.

To Patrícia Vieira for her radiant and resolute character, which has been an incessant source of motivation throughout my physics degree. A word of appreciation is also due to her parents for their incredible support. And finally, to my parents, my gratitude and respect for encouraging me always to be curious and to go a step further.

Resumo

Apesar de mais de um século de verificação experimental, a teoria da Relatividade Geral não é a teoria final da gravitação uma vez que é incompatível com a teoria quântica. As recentes e próximas deteções de ondas gravitacionais oriundas da fusão e coalescência de sistemas binários de objectos compactos e massivos permitem o acesso à física de altas energias junto do horizonte de eventos de buracos negros, onde os efeitos gravitacionais quânticos presumivelmente surgem.

Em particular, estas perturbações quânticas fariam com que a natureza negra e capacidade totalmente absorvente dos buracos negros ficasse comprometida, tendo como consequência a presença de uma sequência de ecos no estágio do *ringdown* do sinal da onda gravitacional. Sendo assim, é de enorme importância que haja uma forma rigorosa de isolar os ecos do sinal e de extrair a informação quântica de cada um deles.

Neste trabalho apresentamos uma primeira e geral equivalência matemática entre a estrutura refletiva no horizonte e a existência de ecos. Para além disto, propomos uma forma de analiticamente isolar o sinal de cada eco mostrando que se pode escrever na forma de uma série de Dyson, para qualquer potencial efetivo, condições fronteira e fontes.

Como exemplo prático, aplicamos o formalismo para calcular explicitamente os ecos de um modelo brinquedo de uma cavidade imperfeita: um espelho perfeito à esquerda e um potencial delta de Dirac à direita. Os nossos resultados permitem a leitura de uma variedade de caractéristicas já conhecidas de ecos, podendo ser usados na análise de dados e na construção de *templates*.

Os Capítulos 3 e 4 deste trabalho estão contidos no recém-publicado artigo *Characterization of echoes: A Dyson-series representation of individual pulses* na *Physical Review D* [1].

Palavras-chave: Ecos, ondas gravitacionais, buracos negros, horizonte de eventos, Relatividade Geral, série de Dyson.

Abstract

Despite its century-long experimental validity, General Relativity is not the final theory of gravity due to its incompability with quantum field theory. The recent and future detections of gravitational waves coming from the merger and colascence of massive compact binaries allow unprecedented experimental access to the high-energy physics around black hole's event horizons, where quantum gravitational effects are expected to emerge.

In particular, these quantum perturbations would cause the all-absorbing dark nature of black holes to become compromised and a series of echoes in the ringdown stage of the gravitational wave signal would necessarily be present. It is thus of enormous relevance to have a rigorous way of isolating echoes from the signal and further extract the quantum information from them.

Here we establish a first, general, mathematical connection between the reflecting structure at the horizon and the existence of echoes. Furthermore, we analytically isolate each echo waveform and show that it can be written in the form of a Dyson series, for arbitrary effective potential, boundary conditions and sources.

As a practical example, we apply the formalism to explicitly determine the echoes of a toy model lossy cavity: a perfect mirror on the left and a Dirac delta potential on the right. Our results allow to read off a number of known features of echoes and may find application in the modelling for data analysis.

Chapters 3 and 4 are contained in the recently published by *Physical Review D* paper *Characterization of echoes: A Dyson-series representation of individual pulses* [1].

Keywords: Echoes, gravitational wave, black hole, event horizon, General Relativity, Dyson series.

Nomenclature

Abbreviations

BC Boundary condition.

BH Black hole.

ClePhO Clean photosphere object.

ECO Exotic compact object.

GR General Relativity.

GW Gravitational wave.

LIGO Laser Interferometer Gravitational-Wave Observatory.

QNM Quasinormal mode.

Symbols

ω Frequency.

Ψ Time-dependent solution of the wave equation.

$\tilde{\Psi}$ Laplace transform of Ψ.

g Green's function of the free wave equation.

I Source term of the wave equation.

R Reflection coefficient.

r_0 Schwarzschild radius.

V Potential of the wave equation.

Contents

Acknowledgments . . . iii

Resumo . . . v

Abstract . . . vii

Nomenclature . . . ix

List of Figures . . . xiii

1 Introduction **1**

1.1 Setup . . . 1

1.1.1 Wave Equation . . . 1

1.1.2 Boundary Condition . . . 2

1.1.3 Potential . . . 2

1.1.4 Echoes . . . 3

1.2 Motivation . . . 4

1.2.1 Black holes, quantum gravity and echoes . . . 4

1.2.2 Quantum mechanical scattering and the key idea herein . . . 6

1.3 State of the Art . . . 8

1.4 Thesis Outline . . . 9

2 Waves in Schwarzschild geometry **11**

2.1 Scalar perturbation . . . 12

2.2 Electromagnetic perturbation . . . 13

2.2.1 Vector spherical harmonics . . . 13

2.2.2 Obtaining the wave equation . . . 14

2.3 The Regge-Wheeler equation . . . 15

2.3.1 Boundary Conditions . . . 16

2.3.2 QNMs and solution . . . 17

3 A Dyson series representation of Echoes **21**

3.1 Boundary Conditions . . . 21

3.2 The Dyson series solution of the Lippman-Schwinger equation . . . 22

3.3 Resummation of the Dyson series and echoing structure . . . 23

3.4 Inversion into the time domain . . . 26

3.5 Reflectivity series . . . 27

4 Echoes of a Membrane-Mirror cavity **31**

4.1 Open system solution: Ψ_o . . . 31

4.2 Echoes: Ψ_n . . . 32

4.3 QNMs . . . 34

5 Conclusions **37**

5.1 Results and achievements . . . 37

5.2 Future developments and work to be done . . . 38

Bibliography **39**

A Generalized Frobenius approach to the Regge-Wheeler equation **41**

B Quasinormal modes **45**

B.1 Sturm-Liouville theory in open systems . . . 45

B.2 Dirac delta spectrum . . . 47

B.2.1 Single Dirac delta . . . 47

B.2.2 Delta & mirror . . . 47

B.2.3 Two deltas . . . 48

B.3 Rectangular barrier spectrum . . . 49

B.3.1 Single barrier . . . 49

B.3.2 Barrier & mirror . . . 51

List of Figures

1.1 Scattering of a narrow gaussian pulse of height 1 observed at $x = 10$, against potential (1.7), a Dirichlet BC at $x = -10$ and an open BC at $x = \infty$. 3

2.1 Regge-Wheeler potential, Eq. (2.31), for $M = 1$, $l = 2$ and $s = 0$ (black), $s = 1$ (red), $s = 2$ (blue). 16

2.2 Time-domain response, $\Re\Psi(t)$, for photon with $l = 5$ and $M = 1$ 19

2.3 Quasinormal behaviour for photon with $l = 5$ and $M = 1$. $\omega = 1.0097 - i\,0.1152$. 20

2.4 Lossy cavity composed by an infinite wall at $x = -50$, extermely close to the horizon, and the Regge-Wheeler potential (2.31) for $M = 1$, $l = s = 2$. The initial wave (black) will enter into the cavity and scatter back and forth between the wall and the potential (blue), but for every collision with the photosphere an *echo* is transmitted (red). 20

4.1 Snapshots of the scalar profile at $t = 0, 6, 10.5, 16, 20, 28, 36, 58, 74$ (top to bottom, left to right) in the presence of a delta-like potential at $x = 0$ and a mirror at $x = -10$. The initial profile (4.16) quickly gives way to two pulses traveling in opposite directions at $t = 6$, as described by Eq. (3.27); the left propagating pulse interacts with the (delta) potential at $t = 10.5$ and gives rise to a transmitted pulse and a reflected one ($t = 16$). The reflected pulse eventually reaches the boundary, at $t = 20$, and will cross the potential at around $t = 36$ giving rise to the first echo. The wave confined to the cavity (mirror+potential) will produce all subsequent echoes. At $t = 58$, after $2L = 20$ time units the second echo emerges out of the cavity and at $t = 74$ a third echo is about to be produced. These snapshots were obtained by adding three "echoes," and coincides up to numerical error, with the waveform obtained via numerical evolution of the initial data. In the central panel, the red line shows $-e^{V_0(x-10)}$, confirming that the initial decay is described by the QNMs (4.5) of the pure delta function (no mirror). 35

4.2 QNM frequencies of the membrane-mirror system for different values of $V_0L = 1, 2, 4, 8$ from bottom (blue) to top (red), respectively. 36

4.3 Time evolution of the waveform using initial conditions (4.16) and parameters (4.17). The plot shows the decay with the fundamental mode of the system (with mirror on the left), $\Im\omega_{\pm 1} \approx -0.00205$ (in red), for large t. The early echoes decay in a way that is governed by the QNMs of the *pure* delta. The high-frequency component is filtered out and progressively the signal is described by the modes of the composite system at late times, as it should. 36

B.1 QNM frequencies for the free case for different values of $V_0a^2 = 1, 2, 4, 8, 16$ from top (black) to bottom (orange), respectively. 51

B.2 QNM frequencies for the mirror case with $L = a$ for different values of $V_0a^2 = 1, 2, 4, 8, 16$ from top (black) to bottom (orange), respectively. 53

B.3 QNM frequencies for the mirror case with $V_0a^2 = 64$ for different values of $L/a = 1, 2, 3, 4, 5$ from top (black) to bottom (orange), respectively. 53

B.4 Quasinormal transition for $V_0a^2 = 64$ and $L = 2a$. The transition occurs for the mode $\bar{n} \approx 12.7324$ with $\Re\omega_{\bar{n}}a \approx \sqrt{V_0a^2} = 8$. 54

Chapter 1

Introduction

***Echo**: the repetition of a sound caused by reflection of sound waves.*

A familiar concept to every individual is the notion of an *echo*. The experience of hearing one's voice over and over in a basement or on a mountaintop is easily a relatable one. It is nevertheless remarkable our brain's capability in segmenting the continuous and smoothly travelling sound wave and further recognizing, in these individualized pulses, the pattern of the original source sound.

The main purpose of this work is to tackle the complexity of this problem by providing a first and mathematically rigorous definition of *echo* in terms of all the relevant physical actors. Luckily, we don't need many ingredients to start aproaching this problem.

1.1 Setup

1.1.1 Wave Equation

The first step should be to define concepts such as *wave* and *reflection* in scientific terms. Take a wave on a string travelling with unitary velocity to the right. If we take a snapshot of the string we can represent its height as a function $\Psi(x)$, where x is the point on the string. After Δt seconds we take another snapshot, the wave moves to the right and we find out that the new amplitude respects $\Psi'(x) = \Psi(x - \Delta t)$. In other words, free wave motion after Δt units corresponds to a *translation* of Ψ by $-\Delta t$. If the wave was travelling to the left, then the translation should be by $+\Delta t$. Thus, we can define a free *wave*, in one spatial dimension, by satisfying

$$\Psi(t, x) := \Psi(x \pm t)\,, \tag{1.1}$$

so that it respects $\partial_x \Psi = \pm\,\partial_t \Psi$ and, applying an extra derivative to get rid of $(\pm)$,

$$\frac{\partial^2 \Psi}{\partial x^2} = \frac{\partial^2 \Psi}{\partial t^2}\,, \tag{1.2}$$

the *wave equation*. Any free *wave*, must be a solution of this equation.

1.1.2 Boundary Condition

Now, what do we understand by *reflection*? Let us consider a left-travelling wave ($\Psi_0(x+t)$) about to hit a wall. The reflected wave Ψ_r will surely be travelling to the right and, by experience, it should have the same shape and resemble Ψ_0. Hence, we can write generically

$$\Psi_r(t,x) = a\,\Psi_0\big(b(x-t)+c\big)\,, \tag{1.3}$$

where a, b and c should be determined by the characteristics and reflective properties of the wall.

Let us go a step further and consider the wall to be at $x=-L$ and be perfectly reflecting. This means that the energy contained in the initial sound wave Ψ_0 will be integrally conveyed into the reflected wave Ψ_r so that, by energy conservation, no sound waves can actually penetrate into the wall, that is $\Psi(t, x \leq -L) := 0$. This establishes the first *boundary condition* of Eq. (1.2). For $x \geq -L$ we also know that the complete wave and solution Ψ of Eq. (1.2) must be the sum of Ψ_0 and Ψ_r, so that, at $x=-L$ we must have

$$0 = \Psi_0(t,-L) + \Psi_r(t,-L) = \Psi_0(-L+t) + a\,\Psi_0\big((c-bL)-bt\big)\,, \tag{1.4}$$

which, for arbitrary Ψ_0 and t, is satisfied for $a=b=-1$ and $c=-2L$, so that the complete solution is given by

$$\Psi(t,x) = \Psi_0(x+t) - \Psi_0\big(-x+(t-2L)\big)\,. \tag{1.5}$$

Note that the reflected wave has a time difference of $2L$ with respect to the initial wave, the same kind of delay found in consecutive *echoes*.

This seems to explain why we keep hearing ourselves inside a large basement (large in the sense $L \gg c\tau$, where τ is the time resolution of the human ear and c the speed of sound), but it does not seem to explain the echoes heard on a mountaintop where sound scatters back and forth across the mountains. In the latter case there is a non-trivial spatial structure that can't be reduced to a set of boundary conditions.

1.1.3 Potential

So, how do we include *structure* into our formalism? We have already done so when considering the wall at $x=-L$, but as a boundary condition, an addendum to the wave equation. We can, however, incorporate the wall directly into the wave equation, by generalizing Eq. (1.2) to

$$\frac{\partial^2\Psi}{\partial x^2} - \frac{\partial^2\Psi}{\partial t^2} = V(x)\Psi\,, \tag{1.6}$$

with $V(x)=0$ if $x>-L$, in which case we recover Eq. (1.2), and $V(x)=\infty$ if $x \leq -L$, such that, if we divide the above by $V(x)$, we get the boundary condition, $\Psi(t,-L)=0$. The plot of $V(x)$ resembles a tall wall located at $x=-L$, i.e. it encodes the structure of the system. It is also clear that a two-wall system, a container, would correspond to a $V(x)$ with two "infinite walls". Thus, to each different system corresponds a profile $V(x)$ that fully characterizes its structure.

A simple model that we will extensively consider in this work is a membrane system, that can be represented by the Dirac delta potential,

$$V(x) = \delta(x) = \begin{cases} \infty & \text{if } x = 0 \\ 0 & \text{if } x \neq 0 \end{cases} . \tag{1.7}$$

Another, more interesting example, which will be deduced from General Relativity in the next chapter, is the Regge-Wheeler potential (in natural units),

$$V(r) = \Big(1 - \frac{2M}{r}\Big)\Big(\frac{l(l+1)}{r^2} + \frac{2M(1-s^2)}{r^3}\Big) , \tag{1.8}$$

where r is the radial coordinate.

1.1.4 Echoes

With the potential $V(x)$ in hand, together with the boundary conditions, we just need to specify the initial wave Ψ_0 to obtain the scattered wave Ψ, from solving the generalized wave equation (1.6). Standard techniques [2] involve a decomposition of Ψ into the natural modes of the system, called *quasinormal modes*, much like a musical note can be decomposed into the specific instrument's harmonics.

If an explicit solution is not attainable, as in the case of most interesting systems, a variety of numerical methods are possible with the aid of techinal computing software like *Mathematica* or *MATLAB*. Either way, the solution is treated as a single mathematical object.

As an example, without going into much detail, below is the plot of a solution Ψ of Eq. (1.6) in a system composed of a membrane alongside a perfectly reflecting wall.

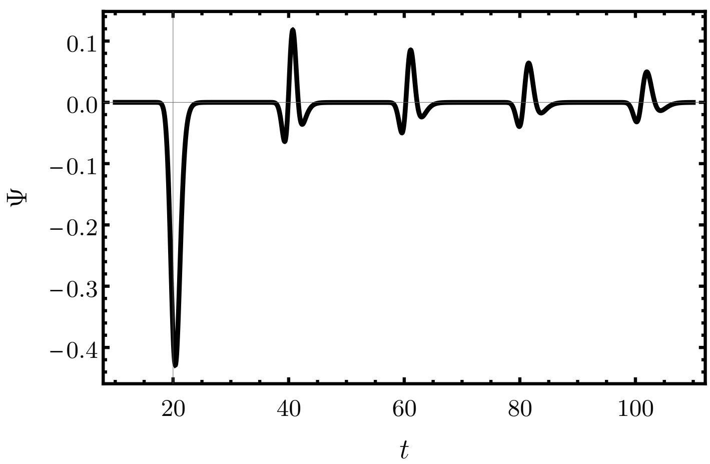

Figure 1.1: Scattering of a narrow gaussian pulse of height 1 observed at $x = 10$, against potential (1.7), a Dirichlet BC at $x = -10$ and an open BC at $x = \infty$.

The bump at $t = 20$ is the reflected pulse off the membrane. It's negativity can be traced back to the $(-)$ sign before the reflected wave in Eq. (1.5). The membrane is not a perfect mirror, however: a portion of the pulse penetrates into the lossy cavity composed of the membrane and the wall. This piece of energy will scatter back and forth inside the cavity, but for every round trip it will leak through the membrane and produce the *echoes* that we see in Figure 1.1.

Obviously, this is our physical intuition working on understanding the physical phenomenon, that the mathematical structure promptly ignores. Our methods give the full solution Ψ of the wave equation, which, due to the strucutre imposed into the system, has to include equally separated regions of relatively large magnitude that we interpret as *echoes*.

Thus, we ask if it is possible to write our solution in the form

$$\Psi = \sum_n \Psi_n \tag{1.9}$$

with Ψ_n the waveform of the n-th *echo*.

In other words, is there a way to mathematically separate the solution of the wave equation (1.6) into a set of functions that we interpret as *echoes*?

The answer is a resounding yes and will be the main topic of this work. It is not surprising that this problem has only been aproached in the last couple of years. This is due to the fact that its solution, with the recent unprecedented detection of gravitational waves [3], will most certainly play a key role on understanding what structure (if any) lies just outside a black hole's event horizon. This might reveal, for the first time in more than a hundred years of experimental validity, what is beyond Einstein's theory of General Relativity.

1.2 Motivation

1.2.1 Black holes, quantum gravity and echoes

A year after Einstein presented the final form of his field equations for gravity in 1915, Karl Schwarzschild found the first non-trivial exact solution of General Relativity (GR), the Schwarzschild metric, which describes the gravitational field outside an uncharged and non-rotating spherical mass. If a spherical mass has a radius smaller than the Schwarzschild radius $r_0 = 2GM/c^2$, the radius from which not even light can escape the gravitational pull, this object is named a black hole (BH).

The spherical region at $r = r_0$, which acts as a one-way membrane and thus causally disconnects the BH interior region from its exterior, is the event horizon. The event horizon protects outside observers from the strongly warped geometry in its interior. This highly energetic region is where quantum gravity effects, not described by Einstein's classical theory of gravity [4], should emerge. Since we only have access to $r > r_0$ we have to consent to look for quantum signs at $r \sim r_0$. In case these are present the all-absorbing property of event horizons becomes altered and a different type of boundary condition, other than a purely ingoing wave, is expected at the event horizon.

Opportunely, we have recently been granted experimental access to the physics around horizons with the historical detections by aLIGO [3, 5] of gravitational waves (GWs) produced by inspiralling binaries of compact objects, the most energetic events registered to date. The GW signal from these systems can be separated in three stages: the inspiral, when the two bodies are still largely separated and possess almost

Newtonian orbits; the merger, when the coalescence occurs; and finally, the ringdown, when the single compact object that results from the collision vibrates and eventually relaxes to a stationary equilibrium solution of GR.

The GWs that come from the last stage, the ringdown phase, originate from the excited space-time near the photosphere $r \sim \frac{3}{2}r_0$ of the final object. However, only the piece that does not fall into the event horizon is capable of being detected in case the merger end-product is a stationary solution of GR - a pure black hole. If non-trivial structure is present near the horizon, *behind* the photosphere, then a portion of the gravitational waves is reflected back from the horizon to the photosphere, which is also able to transmit a fraction of the incident GWs to the far-away observer. Therefore, we can picture a lossy cavity composed of the 'quantum' event horizon and the photosphere, which partially traps gravitational waves and periodically lets loose a fraction of the GWs inside. The end result to the outside observer is the appearance of a series of decaying *echoes* after the main ringdown signal. Hence, it is intuitively clear that detection of echoes in the ringdown signal of future GW observations is synonym with the existence of quantum gravitational effects at the event horizon.

To establish a rigorous and mathematically clear connection between echoes and the hypothetical reflecting structure at horizon is the main motivation behind this work. Previous attempts include some simple models which were employed to claim an important - albeit not enough - statistical evidence for the presence of echoes in the first detections [6–9], a couple of more sophisticated models including BH rotation [10, 11], and the more fundamental work of Mark and collaborators [12] in which the authors were able to isolate the echoes by writing the compact object's Green's function as the BH Green's function plus an additional term responsible by producing the echoes in the complete waveform. Notwithstanding, the latter work assumes the quantum structure to be very close to the horizon - the so-called ClePhOs (Clean Photosphere Objects) - where waves are essentially plane (in the appopriate coordinates). This is not necessarily a drawback given these are the objects whose echoes are expected to appear more separated from each other due to the extreme time dilation at the horizon, and thus benefit greatly from the proposed analytical isolation.

Besides the lack of a completely general framework, there still are a number of open issues regarding the physical behavior of echoes including:

- The completely distinct spectrum of ClePhOs and pure BHs given the exact agreement of both GW signal (only excluding the echoes). Intuitively, the BHs modes should be included in the ClePhOs' spectrum, yet this is not true.

- As in the case of any open system, the very late-time response of ECOs (exotic compact objects) should be governed by the fundamental quasinormal mode. Yet, due to its close relation to BHs, there is some confusion as to whether the fundamental BH QNM might have influence in this decay.

- It is generally accepted that the overall amplitude of sucessive echoes decreases, at least if one is looking for consecutive echoes generated shortly after merger. But what type of decay is this, is it polynomial, exponential? Can we characterize the evolution of echoes in a more precise manner?

- The delay between different echoes is a key quantity in any detection strategy. Is the delay really constant or does it evolve in time, and how [13]?
- In a related vein, a generic widening of the pulses, in the time-domain, was observed as time goes by. This is physically intuitive: the pulses are semi-trapped within a cavity that lets high frequency waves pass. At late times only low-frequency, resonant modes remain. Hence the pulse is becoming more monochromatic. This is an expected but not yet quantified result.
- Consecutive echoes may be in phase or out of phase, depending on the particular boundary conditions imposed on us by the physical model. In particular, what is the relation between the boundary condition imposed at the horizon and the reflecting properties of the quantum structure there?

In this master thesis we will engage in the discussion of these issues. In fact, quickly considering the first point we may wonder whether the usual decomposition in normal modes is the most suitable mathematical approach to isolate the echoes of ClePhOs. Given the large discrepancy with the BH QNM decomposition, we conversely want to find evidence of small decaying repetitions in the wave signal that we see as echoes. 'Small' is the key word here. Perhaps in a perturbative approach, where QNMs are not explicitly taken into account, echoes can be more appropriately mathematically identified. It is thus useful to review the perturbative framework in quantum mechanics, where it was originally developed.

1.2.2 Quantum mechanical scattering and the key idea herein

In quantum mechanics, very few are the systems which are explicitly solvable. In many cases, the potential is seen to have only a slight contribution to the system dynamics, in the sense that observables computed through the free system's eigenfunctions do not differ very much from their real value. Here, first-order perturbation theory comes to the rescue. If the Hamiltonian can be decomposed into a free kinetic term H_0 and a perturbation potential V,

$$H = H_0 + V, \tag{1.10}$$

we might attempt a solution given by the free system explicit solution plus an additional correction:

$$\Psi = \Psi_0 + \Psi_1, \tag{1.11}$$

where Ψ_0 is the explicit solution of the Schrodinger equation, $i\hbar\frac{\partial\Psi_0}{\partial t} = H_0\Psi_0$, and typically corresponds to a simple plane wave (in one spatial dimension).

Now, the full system's Schrodinger equation can be written as

$$\left[i\hbar\frac{\partial}{\partial t} - H_0\right]\Psi_1 = V\Psi_0 + V\Psi_1. \tag{1.12}$$

If V is small when compared to H_0 (and consequently Ψ_1 is small when compared to Ψ_0), then the second term in the rhs is of *second order* and can be neglected under first-order perturbation theory, the so-called Born approximation in scattering theory [14]. In this approximation, the above becomes a solvable differential equation for Ψ_1, given that the lhs is simply the free Schrodinger equation and the rhs is a source term (by construction, the explicit form of Ψ_0 is specified). Thus, taking $V\Psi_1 = 0$ in the above equation gives

$$\Psi_1(x) = \int g_0(x, x')V(x')\Psi_0(x')dx' \tag{1.13}$$

with g_0 the easily obtainable Green's function of the free Schrodinger equation, with the appropriate BCs.

Nonetheless, many systems are not this simple and a first-order correction is often not enough to obtain experimentally and/or numerically acceptable results. If we decide to keep the second-order term $V\Psi_1$ in Eq. (1.12) we can no longer solve for an explicit solution, but will instead obtain an integral equation for Ψ_1, called the Lippmann-Schwinger equation [4], as we'll see in Chapter 3.

The Lippmann-Schwinger equation can be appropriately iterated to obtain further, higher than first, order terms having the form of Eq. (1.13). If the iteration procedure is indefinitely pursued, the resulting infinite summation has the name of *Born series*, and is commonly used in scattering physics - covering optical, molecular, atomic, particle, nuclear and, in this work, also gravitational physics. In quantum field theory, where a closely related perturbation procedure is taken, it has the name of *Dyson series*. Each term of the Dyson series can be associated with a corresponding scattering diagram, or *Feynman* diagram. These diagrams are widely used to compute increasingly precise quantum corrections to collision processes described by the Standard Model. In particular, the most accurate prediction in the history of physics, the electron's anomalous magnetic moment prediction from QED with an agreement of more than 10 signficant figures with the experimentally measured value [4].

Fortunately, the wave equation (1.6) can also be written in the Lippmann-Schwinger form (Chapter 3) and all the methods from quantum perturbation and scattering theory can be employed. In particular, the solution can be written in the form of a Born/Dyson series. However, each term will not give us an isolated echo right away since even the waveform of a completely open system (with no echoes) will always be an infinite sum of terms. Instead, it is easily seen that each term of a Dyson series corresponds to a specific number of interactions with the potential and thus even the echoes should have their respective Dyson series. Then, how do we proceed to identify the echoes contribution in the complete waveform?

We know for sure that the early, pure black hole, response and the echoes are contained in the complete Dyson series. Hence, the first thing to be done is to separate the open BH waveform from the complete waveform, as we then know for sure that the remaining terms will be the joint contribution of all the echoes. This task is relatively easy to perform since the pure BH waveform can also be written in the form of a Dyson series and thus we only need to compare both and see where the latter is contained in the former.

With the echoes all scrambled in the remaining terms we will further need to find a way to identify and isolate each echo contribution. The simple but crucial idea that possibilitated this work consists in noting that the first echo was reflected once at the horizon, the second echo got reflected twice, the third echo thrice, and so on and so forth. This implies that if the quantum wall has a reflection coefficient R, echo number n will carry a factor of R^n. Hence, to isolate the n-th echo contribution we just have to collect the powers of R^n in the remaing terms and effectively *re-sum* the Dyson series into the form (1.9).

In Chapter 3 (or in section II of our paper [1]) this is done in careful detail.

1.3 State of the Art

In this section we review the current stage of research and other developments relevant to the topic of this work. We find it more efficient to provide the reader with a timeline of the most pertinent works that, in our point of view, had direct influence to the topic at hand. We will follow closely section 1.1 of reference [15], which provides a very complete ”roadmap” of the events that shaped GW and QNM research, and add more recent echo related works.

- 1957 - Regge and Wheeler [16] show ”that a Schwarzschild singularity, spherically symmetrical and endowed with mass, will undergo small vibrations about the spherical form and will therefore remain stable if subjected to a small nonspherical perturbation”. This marks the birth of BH perturbation theory.

- 1970 - Zerilli [17] extends the Regge-Wheeler analysis to general perturbations of a Schwarzschild BH. He shows that the perturbation equations can be reduced to a pair of Schrödinger-like equations, and applies the formalism to study the gravitational radiation emitted by infalling test particles.

- 1970 - Vishveshwara [18] studies numerically the scattering of gravitational waves by a Schwarzschild BH: at late times the waveform consists of damped sinusoids

- 1971 - Press [19] identifies ringdown waves as the free oscillation modes of the BH.

- 1971 - Davis [20] carry out the first quantitative calculation of gravitational radiation emission within BH perturbation. Quasinormal ringing is excited when a radially infalling particle crosses $r \sim \frac{3}{2}r_0$ (i.e., close to the unstable circular orbit corresponding to the “light ring”).

- 1975 - Chandrasekhar and Detweiler [21] compute numerically some weakly damped characteristic frequencies. They prove that the Regge-Wheeler and Zerilli potentials have the same spectra.

- 1985 - Leaver [22–24] provides the most accurate method to date to compute BH QNMs using continued fraction representations of the relevant wavefunctions, and discusses their excitation using Green’s function techniques.

- 1992 - Nollert and Schmidt [25] use Laplace transforms to compute QNMs.

- 1997 - Maldacena [26] formulates the Ads/CFT duality conjecture. This opens up the range of applicability of QNM research.

- 2005 - Pretorius [27] (and other groups later) achieve a long-term stable numerical evolution of a BH binary. The waveforms indicate that ringdown contributes a substantial amount to the radiated energy.

- 2009 - A review on QNMs [15], with a focus on the most recent developments, by Berti, Cardoso and Starinets.
- 2016 - Gravitational waves are detected for the first time by LIGO [3, 5]. The signal matches the waveform predicted by general relativity for the inspiral and merger of a pair of black holes and the ringdown of the resulting single black hole.
- 2016 - The suggestion that quantum effects might destroy the event horizon. It was thought that if the horizon did not exist then the final stage of coalescence would be completely different. This would imply that LIGO discovery was evidence of the existence of BH [6, 28, 29].
- 2017 - A tentative (and somewhat controversial [8, 9]) evidence at $\approx 3\sigma$ confidence level was found for the presence of echoes in the three first black hole merger events detected by LIGO: GW150914, GW151226, and LVT151012 [6, 7].
- 2017 - A first mathematical description of echo identification from exotic compact object's response was proposed by Z. Mark and collaborators at TAPIR in Caltech [12].

1.4 Thesis Outline

The preparation material studied in the *Project MEFT* course and the early stages of this dissertation is condensed into Chapter 2. In this chapter the wave equation in a Schwarzschild background for both massless scalar waves (Section 2.1) and photons (Section 2.2) is deduced. In Section 2.3 we apply a boundary expansion to numerically solve this equation and obtain the waveform of a scattered electromagnetic Gaussian wavepacket off a Schwarzschild BH. A closer look at the ringdown stage allows inspection of the fundamental, least damped, QNM.

It is in Chapter 3 that the perturbative approach to gravitational wave scattering is taken. We start with a proper consideration of the BC at the horizon and its relation with the reflection coefficent (Section 3.1). Then, the Lippmann-Schwinger equation and corresponding Born/Dyson series is adapted to our generalized BC choice (Section 3.2) in order to be resummed and separated into isolated echoes, besides the early open system response (Section 3.3). In Section 3.4, the inverse Laplace transform allows the obtention of the wave equation final solution, the time-dependent waveform. However, since the latter procedure is only possible in case the reflection coefficient at the horizon is explicitly known, we further propose a perturbative method to derive it in Section 3.5. This chapter corresponds to section II in our paper [1].

In Chapter 4, we apply the previous chapter apparatus to determine the echoes of a membrane-mirror cavity (a perfectly reflecting mirror at the left and a partially transmissible Dirac delta potential at the right). Given the explicit attainability of the final solution there is no need to truncate the Dyson series of neither the open system waveform (Section 4.1) nor the echoes (Section 4.2). We also find interesting to apply the results in Section 3.5 to determine the reflectivity of the whole system (Section 4.3), which confirms the different spectrum between composite and pure systems (also seen in Section B.2 but through a different method). This chapter corresponds to section III in our paper [1].

We conclude with a review of the main topics covered in this work. Additionally, we elaborate on future prospects, possible developments of the ideas presented, and the impact our work can have in GW research and other areas.

Both of the appendices consist of early original work not directly related to echoes, even if relevant in the context of this thesis. Appendix A is useful to understand why a numerical approach is necessary to solve the Regge-Wheeler equation. We employed the Frobenius method [2] with a free boundary behavior. By appropriately fixing the BC, we are able to see that the most simplified solution is Leaver's 3-term recursion relation [22] which is currently the prime method for QNM computation.

Appendix B consists of a proper mathematical definition of quasinormal modes supplied by a proof of the equivalence between open systems and the dissipation of waves within, in section B.1, and further numerical and explicitly approximate determination of the QNMs of the Dirac delta potential (Section B.2) and the Rectangular potential barrier (Section B.3) with a variety of boundary conditions.

Chapter 2

Waves in Schwarzschild geometry

In section 1.1 we defined the concept of wave as formally being a solution of the generalized wave equation (1.6). We have used the example of waves on a string, but waves have many types and origins. String and sound waves propagate due to mechanical interaction of the molecules that constitute the medium, and are thus able to propagate both transversally and longitudinally. Hence, in Eq. (1.6), Ψ more suitably corresponds to one of the 3 components of these *vectorial* waves.

Here we'll consider more fundamental waves which, through the wave-particle duality, correspond to elementary particles and thus do not require a physical medium of propagation. More specifically, we will take a generic massive scalar boson and the electromagnetic force carrier, the *photon*, a two-polarization vector field.

It is also important to note that Eq. (1.6) is a linear differential equation, which for most realistic cases only holds at a first approximation level. This is because interactions between fields necessarily include at least a quadratic term in the equations of motion that quickly turn them into unsolvable partial differential equations, hence the usefulness of linearizing the wave equation.

In this approximation, the Einstein field equations simplify greatly since the energy-momentum tensor, which is the source of space-time curvature, vanishes due to its quadratic dependence on the matter fields. Therefore, the linearized perturbations do *not* create any gravitational field nor affect the background geometry, which we will take to be the Schwarzschild geometry.

The Schwarzschild solution of General Relativity describes the space-time curved by a static point particle of mass M (at the origin) through the metric, in the usual spherical coordinates, given by

$$g_{\mu\nu} = \mathrm{diag}\big(-f, f^{-1}, r^2, r^2 \sin^2\theta\big), \tag{2.1}$$

with

$$f = 1 - \frac{2M}{r}, \tag{2.2}$$

which diverges at $r = 2M$, the black hole event horizon.

Now, we just have to solve the free wave equation with the prescription $\partial_\mu \to \nabla_\mu$, where ∇_μ is the covariant derivative associated with the metric (2.1). We will see that potential (1.8) will arise naturally, and interestingly will depend on the specific choice of perturbation.

2.1 Scalar perturbation

The evolution of a scalar field Φ of mass m is determined by its wave equation, the Klein-Gordon equation, in Schwarzschild spacetime,

$$\nabla_\mu \nabla^\mu \Phi = \partial_\mu(\sqrt{-g}\, g^{\mu\nu}\partial_\nu \Phi) = m^2 \Phi \tag{2.3}$$

which by imput of metric (2.1) yields

$$-\sin\theta\, \frac{r^2}{f}\, \frac{\partial^2 \Phi}{\partial t^2} + \sin\theta \frac{\partial}{\partial r}\Big(r^2 f \frac{\partial \Phi}{\partial r}\Big) + \frac{\partial}{\partial \theta}\Big(\sin\theta \frac{\partial \Phi}{\partial \theta}\Big) + \frac{1}{\sin^2\theta}\frac{\partial^2 \Phi}{\partial \varphi^2} = m^2 \Phi\,. \tag{2.4}$$

Employing a separation of variables in the form $\Phi(r,t,\theta,\varphi) = T(t)\,\phi(r,\theta,\varphi)$, we obtain

$$\frac{T''}{T} = \frac{f}{r^2 \phi}\bigg(\frac{\partial}{\partial r}\Big(r^2 f \frac{\partial \phi}{\partial r}\Big) + \frac{1}{\sin\theta}\frac{\partial}{\partial \theta}\Big(\sin\theta\, \frac{\partial \phi}{\partial \theta}\Big) + \frac{1}{\sin^2\theta}\frac{\partial^2 \phi}{\partial \varphi^2}\bigg) - m^2 = -\omega^2 \tag{2.5}$$

where $\omega \in \mathbb{C}$ must be a constant, so that the time dependence has the plane wave form $T \sim e^{\pm i\omega t}$.

Further writing $\phi(r,\theta,\varphi) = R(r)Y(\theta,\varphi)$ makes the above simplify to

$$\frac{(r^2 f R')'}{R} + \frac{(\omega^2 - m^2)r^2}{f} = -\frac{1}{Y}\bigg(\frac{1}{\sin\theta}\frac{\partial}{\partial\theta}\Big(\sin\theta\,\frac{\partial Y}{\partial\theta}\Big) + \frac{1}{\sin^2\theta}\frac{\partial^2 Y}{\partial\varphi^2}\bigg) = \lambda \tag{2.6}$$

where $\lambda = l(l+1)$, with $l \in \mathbb{N}$.

The angular part of the above equation is nothing but the *spherical harmonics* equation. In other words, $Y \sim Y_{ln}$, the spherical harmonic function of degree l and order n.

In fact, we could have started by decomposing Φ into spherical harmonics since we setup our coordinate system to be centered at the static point-mass M which naturally deforms space-time isotropically. It is easy to see that the Schwarzschild metric (2.1) exhibits spherical symmetry.

We proceed by writing $R = \psi/r$ to get the final form of the wave equation:

$$f^2\psi'' + f f'\psi' + (\omega^2 - V)\psi = 0 \tag{2.7}$$

with effective potential

$$V(r) = m^2 - \frac{2Mm^2}{r} + f\Big(\frac{l(l+1)}{r^2} + \frac{f'}{r}\Big), \tag{2.8}$$

where m^2 is the rest mass contribution to the energy, $-\frac{2Mm^2}{r}$ can be associated to Newtonian-like gravitational attraction, and finally the factor of f, which individually accounts for relativistic effects near the horizon, that includes the centrifugal barrier, $\frac{l(l+1)}{r^2}$, coming from spherical harmonic decomposition and the term $\frac{f'}{r}$ which we cannot yet interpret.

2.2 Electromagnetic perturbation

The source-free Maxwell's equations in a curved background hold as

$$\nabla_\nu F^{\mu\nu} = \frac{1}{\sqrt{-g}}\partial_\nu(\sqrt{-g}F^{\mu\nu}) = 0, \tag{2.9}$$

with

$$F_{\mu\nu} = \nabla_\mu A_\nu - \nabla_\nu A_\mu, \tag{2.10}$$

where A_μ is the photon field.

We could begin by attempting a variable separation, like we did for the scalar case. However, we would have to handle 4 coupled equations (the index μ is not contracted) in all 4 coordinates. Moreover, since a non-rotating black hole is spherically symmetric, a spherical harmonic decomposition should be possible right from the start. But should we assume $A_\mu(\theta,\phi) \sim Y_{ln}$, i.e. that the 4 components of the angular dependence of the photon field behave as 4 independent scalar fields under rotations?

If we picture a longitudinal wave in a spring and perform a rotation on its axis we will see that indeed the system will remain the same. But if we do the same rotation for a transversal wave on a string it is clear that the oscillations will acquire a different angle on that axis, if the rotation is not by a multiple of 2π. Thus, we intuively understand that longitudinal and transversal modes *transform* differently under rotations, and that the previous assumption was too naive.

At a mathematical level, this means that a variable separation will not lead to the *scalar* spherical harmonic equation (2.6), but to a matrix version of (2.6) which includes the vector rotations. We can, nevertheless, circumvent this trouble by looking for the associated expansion in *vector spherical harmonics*.

2.2.1 Vector spherical harmonics

We start by noting that spherical harmonics are eigenfunctions of the azimuthal rotation generator $\frac{\partial}{\partial\varphi}$ (naturally a *Killing* vector field of the Schwarzchild metric). Now, we must ask ourselves how a vector field changes under azimuthal rotations. Let us take an infinitesimal rotation by $\varphi = \delta\alpha$ so that, in Cartesian coordinates,

$$(t,x,y,z) \to (t, x - y\delta\alpha\,, y + x\delta\alpha, z) \tag{2.11}$$

and

$$\frac{\partial}{\partial x} \to \frac{\partial}{\partial x} + \delta\alpha\,\frac{\partial}{\partial y}\,, \quad \frac{\partial}{\partial y} \to \frac{\partial}{\partial y} - \delta\alpha\,\frac{\partial}{\partial x}\,, \tag{2.12}$$

implying

$$\mathbf{A} = A^\mu\partial_\mu \to (1 + i\delta\alpha L_z)A^\mu\,(1 + i\delta\alpha S_z)\partial_\mu = (1 + i\delta\alpha(L_z + S_z))\mathbf{A} \tag{2.13}$$

with

$$L_z = -i\Big(x\frac{\partial}{\partial y} - y\frac{\partial}{\partial x}\Big)\,, \quad S_z = -i\frac{\partial}{\partial z}\times\,, \tag{2.14}$$

the z-components of the operators angular momentum (rotations on the manifold), and spin (rotations on the vector space), respectively. The imaginary unit is required to keep operators hermitian and $\times$ represents the 3-dimensional cross product.

Scalar spherical harmonics are eigenfunctions of angular momentum by respecting Eq. (2.6) that, in operator form, read as $L^2 Y_{lm} = l(l+1)Y_{lm}$, $L_z Y_{lm} = mY_{lm}$. To construct the vector spherical harmonics, we must find the eigenfunctions, more appropriately eigenvectors, of the spin operator $\mathbf{S}$.

It is straightforward to show that the cross product in $\mathbb{R}^3$ can be put in a 3×3 matrix form, implying that S_z has 3 eigenvalues. The eigenvector equation $S_z \mathbf{e}_M = M\mathbf{e}_M$ yields $M = -1, 0, 1$ with

$$\mathbf{e}_{-1} = \frac{1}{\sqrt{2}}\Big(\frac{\partial}{\partial x} + i\frac{\partial}{\partial y}\Big)\,, \quad \mathbf{e}_0 = \frac{\partial}{\partial z}\,, \quad \mathbf{e}_1 = \frac{1}{\sqrt{2}}\Big(\frac{\partial}{\partial x} - i\frac{\partial}{\partial y}\Big)\,, \tag{2.15}$$

respecting $S^2\mathbf{e}_M = 2\mathbf{e}_M = 1(1+1)\mathbf{e}_M$ thereby confirming that photons are indeed spin 1 bosons.

Taking into account the vectorial nature of the photon, Regge and Wheeler, in 1957, proposed an efficient basis [16] for *vector* spherical harmonics by applying the spatial operators directly involved in (2.9), $\mathbf{L}$ and $\boldsymbol{\nabla}$, to the scalar spherical harmonic Y_{lm}, as follows:

$$[Y_{lm}\partial_t] = (Y_{lm}, 0, 0, 0) \tag{2.16}$$

$$[Y_{lm}\partial_r] = (0, Y_{lm}, 0, 0) \tag{2.17}$$

$$[\boldsymbol{\nabla} Y_{lm}] = (0, 0, \partial_\theta Y_{lm}, \partial_\varphi Y_{lm}) \tag{2.18}$$

$$[\mathbf{L}Y_{lm}] = (0, 0, ir\frac{1}{\sin\theta}\partial_\varphi Y_{lm}, -ir\sin\theta\partial_\theta Y_{lm}) \tag{2.19}$$

With this basis we can proceed to simplify Eq. (2.1) to get the wave equation.

2.2.2 Obtaining the wave equation

Luckily, we will not need to handle connection or curvature terms since

$$F_{\mu\nu} = \nabla_\mu A_\nu - \nabla_\nu A_\mu = \partial_\mu A_\nu - \partial_\nu A_\mu \tag{2.20}$$

because of symmetry of the Levi-Civita connection.

We can now decompose A_μ into vector spherical harmonics through the basis (2.16-19) into

$$A_\mu = \sum_{l,m} \begin{pmatrix} a^{lm}(t,r)Y^{lm} \\ b^{lm}(t,r)Y^{lm} \\ c^{lm}(t,r)\partial_\theta Y^{lm} + d^{lm}(t,r)\frac{\partial_\phi Y^{lm}}{\sin\theta} \\ c^{lm}(t,r)\partial_\phi Y^{lm} - d^{lm}(t,r)\sin\theta\partial_\theta Y^{lm} \end{pmatrix}. \tag{2.21}$$

Decoupling all angular dependence of the 4 equations (2.1) using this decomposition yields

$$l(l+1)(a^{lm} - \partial_t c^{lm}) - rf(2\partial_r a^{lm} + r\partial_r^2 a^{lm} - 2\partial_t b^{lm} - r\partial_t\partial_r b^{lm}) = 0 \tag{2.22}$$

$$l(l+1)(b^{lm} - \partial_r c^{lm}) + \frac{r^2}{f}(-\partial_r\partial_t a^{lm} + \partial_t^2 b^{lm}) = 0 \tag{2.23}$$

$$ff'(b^{lm} - \partial_r c^{lm}) + f^2(\partial_r b^{lm} - \partial_r^2 c^{lm}) - \partial_t a^{lm} + \partial_t^2 c^{lm} = 0 \tag{2.24}$$

$$\frac{l(l+1)f}{r^2} d^{lm} - ff'\partial_r d^{lm} - f^2\partial_r^2 d^{lm} + \partial_t^2 d^{lm} = 0 \tag{2.25}$$

where the angular momentum l naturally appears a result of the use of the spherical harmonic Eq. (2.6).

We must now look for the physical, gauge invariant, wave equations. For this we perform $A_\mu \to A_\mu + \partial_\mu\alpha$ which is equivalent to $a^{lm} \to a^{lm} + \partial_t\beta$, $b^{lm} \to b^{lm} + \partial_r\beta$, $c^{lm} \to c^{lm}$, $d^{lm} \to d^{lm}$ for some $\beta(t,r)$ related to $\alpha(t,r,\theta,\phi)$. The latter remain invariant since $\partial_\theta\alpha$ and $\partial_\phi\alpha$ get absorbed into the spherical harmonics equation.

Equation (2.25) only depends on d^{lm}, thus being automatically gauge invariant. Under the gauge transformation, equation (2.22) gets an extra $l(l+1)\partial_t\beta$ in the l.h.s whereas equation (2.23) gets simirilaly added by $l(l+1)\partial_r\beta$. We construct a gauge invariant equation by applying ∂_r to (2.22), ∂_t to (2.23) and subtracting both. The resulting equation has no dependence on c^{lm} and has the same form of (2.25) where d^{lm} gets replaced by the gauge invariant quantity

$$\epsilon^{lm} = \frac{r^2}{l(l+1)}(\partial_t b^{lm} - \partial_r a^{lm})\,. \tag{2.26}$$

It is not difficult to see that c^{lm} can be expressed by some combination of ϵ^{lm} and d^{lm}, the two physical degrees of freedom of the photon field. Equation (2.25) and the equivalent one for ϵ^{lm} can be rewritten in the form

$$f^2\psi'' + ff'\psi' + (\omega^2 - V_{s=1})\psi = 0 \tag{2.27}$$

with

$$V_{s=1}(r) = f\frac{l(l+1)}{r^2} \tag{2.28}$$

where $\psi = d^{lm}e^{i\omega t}$ for odd-parity perturbations and $\psi = \epsilon^{lm}e^{i\omega t}$ for even-parity perturbations.

Notice that the above potential is very similar to the scalar field case, Eq. (2.8), if $m = 0$. The additional term $f\frac{f'}{r}$ thus depends on the choice of perturbation, it is spin-dependent.

Before we proceed, we note that we should expect the same equation for both odd-parity and even-parity perturbations since spherically symmetric interactions have no preference over the orientation of the internal degrees of freedom of the probe field. The same reasoning explains why there is no azimuthal number m dependence in neither of Eqs. (2.27) or (2.28).

2.3 The Regge-Wheeler equation

A way to incorporate both choices of massless perturbations (scalar and vector) into one equation is to write it as

$$f^2\psi'' + ff'\psi' + \Big(\omega^2 - f\Big(\frac{l(l+1)}{r^2} + f'\frac{1-s^2}{r}\Big)\Big)\psi = 0, \tag{2.29}$$

the *Regge-Wheeler equation*, where s is the spin.

For $s = 0$ we recover (2.8) (with $m = 0$) and for $s = 1$ we get back potential (2.28). This specific generalization also importantly describes massless spin-2 fields, which are associated with gravitational perturbations [16].

Now we can use the *tortoise* coordinate x, with $\frac{dr}{dx} = f$, to write the above into the more familiar form

$$\frac{d^2\psi}{dx^2} + \big(\omega^2 - V(x)\big)\psi = 0 \tag{2.30}$$

with potential (1.8), which we repeat here for convenience,

$$V(x) = \Big(1 - \frac{2M}{r(x)}\Big)\Big(\frac{l(l+1)}{r^2(x)} + \frac{2M(1-s^2)}{r^3(x)}\Big), \tag{2.31}$$

with

$$x = r + 2M\log\Big(\frac{r}{2M} - 1\Big). \tag{2.32}$$

The tortoise coordinate respects $x \to \infty \Leftrightarrow r \to \infty$ and $x \to -\infty \Leftrightarrow r \to 2M$. Hence, by using x we are automatically disregarding the causally disconnected region $r < 2M$ when writing the wave equation.

Below is a plot of Eq. (2.31) with respect to the tortoise coordinate. Note the decay $\sim \frac{1}{x^2}$ for large x, reminescent of the centrifugal barrier, and the sharp decay at $x \sim 0$ caused by relativistic effects at the near-horizon region. The maximum of the potential is located at $x \sim 2M$ or $r \sim \frac{3}{2}r_0$, the photosphere, where scattering is more violent.

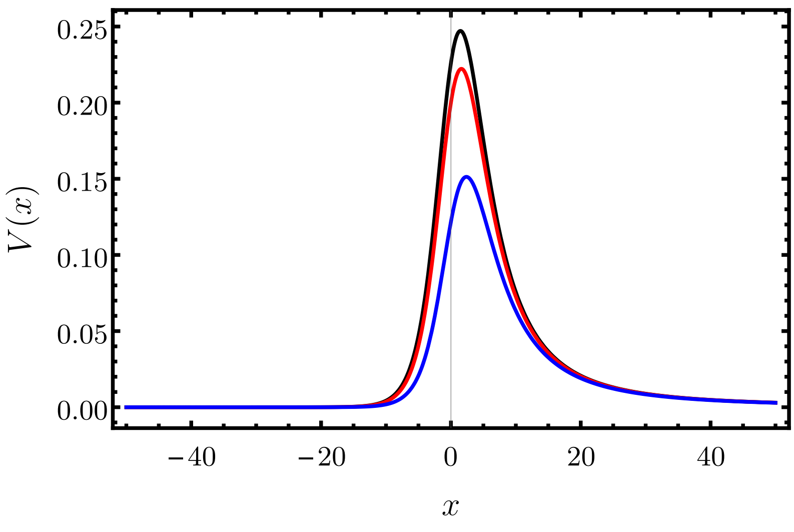

Figure 2.1: Regge-Wheeler potential, Eq. (2.31), for $M = 1$, $l = 2$ and $s = 0$ (black), $s = 1$ (red), $s = 2$ (blue).

2.3.1 Boundary Conditions

To solve Eq. (2.29) we need to specify two boundary conditions. The only structure that we are considering in our system is the point-mass at $r = 0$. Hence, we have a physically open system and thus we should look to behaviour at $x \to \pm\infty$, where the potential (2.31) vanishes and Eq. (2.30) reduces to the free wave equation. By noting that the time dependence was chosen to be of the form $e^{-i\omega t}$ we have to decide which behaviour, $\psi \sim e^{\pm i\omega x}$, is the appropriate at $x \to \pm\infty$.

Now, if we do not want any external influence on the system we can only have outgoing waves at infinity, $e^{i\omega(x-t)}$, and thus the first boundary condition should be

$$\psi(x \to \infty) \propto e^{i\omega x}. \tag{2.33}$$

Furthermore, no waves can escape the event horizon implying that the only physical possibility is to have ingoing waves at $x \to -\infty$, which establishes the second boundary condition,

$$\psi(x \to -\infty) \propto e^{-i\omega x}. \tag{2.34}$$

Note that these boundary conditions necessarily imply that the system is *dissipative*. All waves either flow out to infinity or into the horizon. Hence, contrarily to conservative systems, like a string fixed at both ends, the perturbation Ψ has to decay in time. For the assumed behaviour $\Psi(t,x) = e^{-i\omega t}\psi(x)$, this implies that ω *cannot* be a pure real number, it has to have a non-zero and negative imaginary part, so that $\Psi \sim e^{-|\Im\omega|t}$ (for a rigorous proof we refer to Appendix B.1). These complex frequencies have the name of *quasinormal modes* and are ubiquitous in every field of physics.

2.3.2 QNMs and solution

To extract the black hole quasinormal spectrum we have to solve Eq. (2.29) with boundary conditions (2.33) and (2.34). Unfortunately, this is not possible to do analytically (see Appendix A). A numerical approach is necessary, which we employ here. We try to avoid the mathematical details, which are appropriately considered in Appendix A.

To get a numerically efficient way to solve Eq. (2.29) one should bring the boundary conditions "closer" to one another by series expansions at the boundaries. At $r \to \infty$ we write

$$\psi(r) = e^{i\omega r} \sum_{n=0}^{\infty} B_n \, r^{-n}, \tag{2.35}$$

where $e^{i\omega r}$ captures the correct boundary condition, i.e. it is recovered in the above expansion when $r \to \infty$ since only the $n = 0$ term survives. It is clear that the remaining terms become more relevant as soon as we bring r to smaller values, effectively bringing the boundary condition at ∞ closer to numerically acceptable boundary values of r. This effect is greater the higher the truncation order of the expansion is.

Insertion of (2.35) into (2.29) turns the ODE into the recursion relation

$$\begin{aligned}
&B_n\big(2in\omega\big)\\
&+ B_{n-1}\big(-l(l+1) + (n-1)(n-2ir_0\omega)\big)\\
&+ B_{n-2}\, r_0\big(l(l+1) - 3(n-2) - 2(n-2)^2 - 1 + s^2\big)\\
&+ B_{n-3}\, r_0^2\big(2(n-3) + (n-3)^2 + 1\big) = 0,
\end{aligned} \tag{2.36}$$

where $B_{n<0} = 0$. All the coefficients can thus be recursively computed, except for B_0, which is an arbitrary constant that can be fixed by a second boundary condition at $r \to \infty$.

The recursion relation for $r \to 2M$ is similar and is done in Appendix A. Now, one possible way to proceed is by direct integration [30], which essentially consists of a couple of numerical integrations: From the horizon to some matching point r_m imposing the ingoing boundary condition (2.34), and from infinity to r_m imposing the outgoing boundary condition (2.35). Then, conditions $\psi(r_m^-) = \psi(r_m^+)$ and $\psi'(r_m^-) = \psi'(r_m^+)$ are only satisfied for a discrete set of QNM frequencies ω, which then become automatically determined. The disavantage is that a high truncation order (~ 10) of the expansion (2.35) is required.

The method we apply here presents satisfactory results for a truncation order ~ 3. The problem of computing the gravitational waveform produced when a black hole is perturbed by some material source can be reduced to the inhomogeneous version of Eq. (2.29), where a source term $I(\omega, r)$ is included at the *rhs* [2].

The Green's function approach [2] allows us to write the frequency amplitude in terms of the source term as

$$\Psi(\omega, r) = \int_{2M}^{\infty} G(r, r')\, I(\omega, r')\, dr', \tag{2.37}$$

where the Green's function can be computed through the expression

$$G(r, r') = \frac{\psi_L\big(\min(r, r')\big)\psi_R\big(\max(r, r')\big)}{W}, \tag{2.38}$$

with the Wronskian given by $W = \psi_R'\psi_L - \psi_L'\psi_R$, and ψ_L an homogeneous solution of (2.29) respecting the boundary condition at the left (2.34) and equivalently ψ_R obeying the boundary condition at the right (2.33). Note that ψ_L and ψ_R only obey both boundary conditions for very specific values of ω, the quasinormal frequencies, where also the Wronskian vanishes and $G(r, r')$ diverges. In other words, the poles of the Green's function constitute the quasinormal spectrum. This result is general, even for conservative systems where the spectrum sits on the real line.

With the homogeneous solutions ψ_L, ψ_R obtained numerically using *Mathematica* supplied by the "near" boundary expansions (2.35) and (A.9) we are now interested in knowing the solution at infinity, where gravitational waves are observed, for all practical purposes. Performing the limit $r \to \infty$ allows to write

$$\Psi(\omega, r \to \infty) = \frac{e^{i\omega r}}{W} \int_{2M}^{\infty} \psi_L(r')\, I(\omega, r')\, dr', \tag{2.39}$$

using the explicit expression for the Green's function, Eq. (2.38).

Now, to ensure convergence we take a gaussian source term of the form

$$I(\omega, r) = e^{-(x(r) - x_0)^2/\sigma^2}, \tag{2.40}$$

centered at x_0 where we use x, the tortoise coordinate (to make sure all sources are located outside the black hole).

Finally, the time-domain response is obtained by inversion of the Laplace transform:

$$\Psi(t,r) = \int_0^\infty \Psi(\omega,r)e^{-i\omega t}d\omega\,. \tag{2.41}$$

Note that at $r \to \infty$, expression (2.39) inserted above implies that $\Psi(t,r) \propto e^{i\omega(r-t)}$, a freely travelling outgoing wave, as it should to be.

This formula, together with Eq. (2.39), allows to compute the wave signal at infinity, $\Psi(t, r \to \infty)$ in function of the source $I(\omega,r)$, which we naturally we expect to be composed of many quasinormal modes with different amplitudes. However, if the modes' imaginary part is non-degenerate (I can't think of any example where this is not the case for dissipative systems), we know that there is one mode that will have the lowest imaginary component, in magnitude, which is usually the *fundamental mode*. Thus, the remaining modes' contribution to $\Psi(t,r)$ will fade out faster and, after a sufficiently long time, we expect the waveform to exclusively vibrate with the less-damped mode. This enables numerical extraction of this mode by fitting this time-region of $\Psi(t,r)$ to a damped sinusoid.

For instance, when $M = 1$, $l = 5$, $s = 1$, $x_0 = \sigma = 10$, the waveform $\Re\Psi(t, r \to \infty)$ at the observer has the following plot.

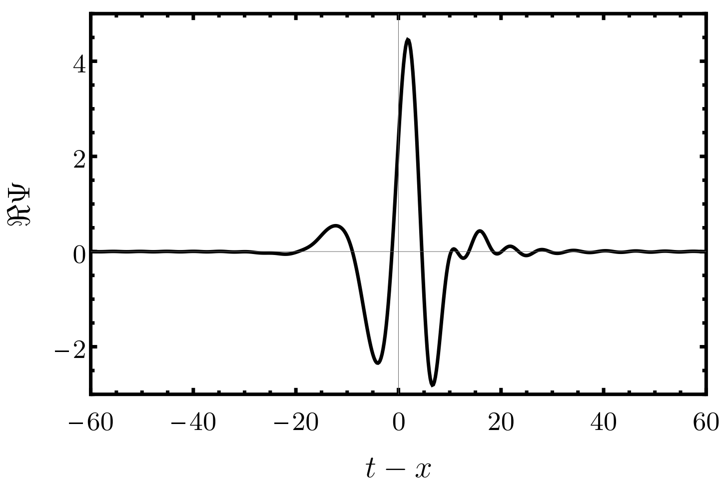

Figure 2.2: Time-domain response, $\Re\Psi(t)$, for photon with $l = 5$ and $M = 1$

We see the low amplitude ringing modes for $t >\sim 20$. A closer look on this region (figure 2) reveals the quasinormal behaviour $e^{-\omega_i t}\sin\omega_r t$ for which the best fit parameters are $\omega_r = 1.0097$, $\omega_i = 0.1152$, in acceptable agreement with the ringdown database from CENTRA [15].

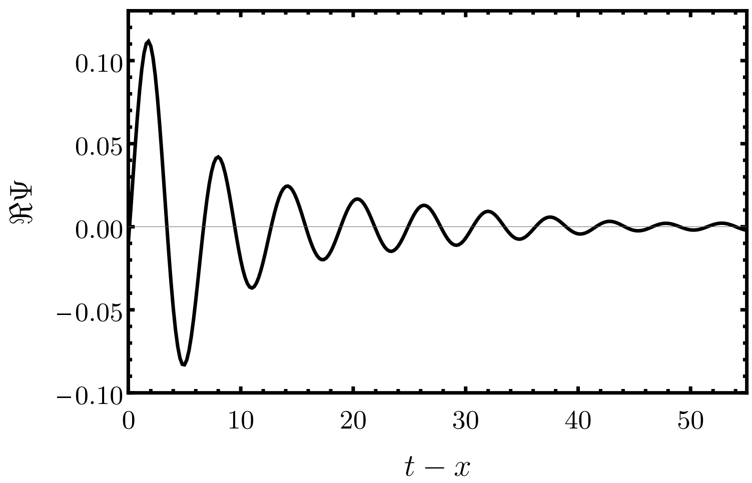

Figure 2.3: Quasinormal behaviour for photon with $l = 5$ and $M = 1$. $\omega = 1.0097 - i\,0.1152$.

This chapter ends the preparation material for next chapter, which kicks off by asking the question: What happens if the boundary condition at the horizon is not simply Eq. (2.34)? If there is some *structure*, of quantum nature perhaps, at the horizon then we should expect some portion of the waves to be reflected back to the light ring, as depicted below. These waves will scatter back and forth, slowly leaking through the photosphere and, as a result, produce echoes in the gravitational wave signal.

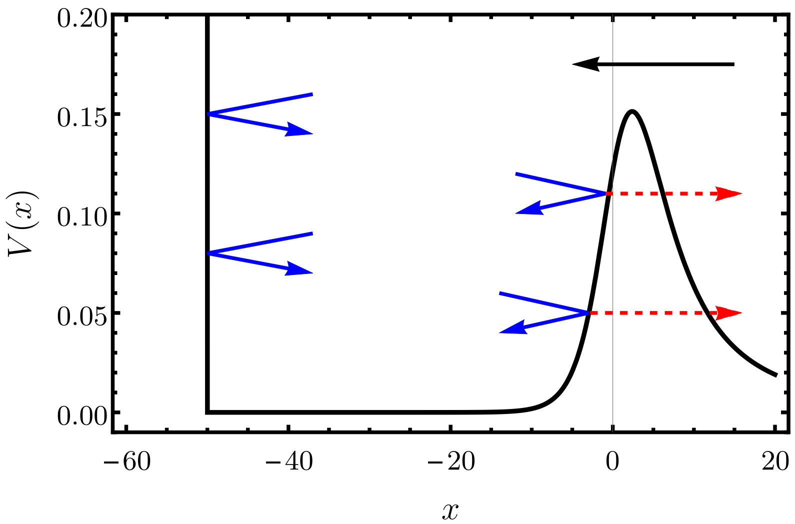

Figure 2.4: Lossy cavity composed by an infinite wall at $x = -50$, extermely close to the horizon, and the Regge-Wheeler potential (2.31) for $M = 1$, $l = s = 2$. The initial wave (black) will enter into the cavity and scatter back and forth between the wall and the potential (blue), but for every collision with the photosphere an *echo* is transmitted (red).

These echoes will individually carry valuable information about the structure at the horizon. Thus, it is of extreme importance to have a mathematical formalism where we can obtain the waveform as a sum of separated echoes. In other words, a general formula for *each* echo would allow us to directly correlate their signal with the reflective properties of the structure at the horizon, and consequently shed a new light on the quantum nature of gravity.

Chapter 3

A Dyson series representation of Echoes

The starting point has to be the wave equation,

$$-\frac{\partial^2\Psi}{\partial t^2}+\frac{\partial^2\Psi}{\partial x^2}-V(x)\Psi=0, \tag{3.1}$$

which, in this chapter, will be appropriately solved through an echo decomposition.

3.1 Boundary Conditions

As we have seen in the last chapter, the boundary conditions have a very relevant influence on the waveform. Here we are particularly interested in partially open systems, where waves can escape to infinity in at least one of the sides, which we will pick to be the right side, $+\infty$, without loss of generality,

$$\Psi(t,x\to\infty)\propto e^{i\omega(x-t)}\,, \tag{3.2}$$

The boundary condition at the left, however, may include a partial reflection at some point $x=-L$,

$$\Psi(t,x\sim -L)\propto e^{-i\omega(x+t)}+R(\omega)\,e^{i\omega(x-t)}\,, \tag{3.3}$$

where the first term corresponds to a free wave travelling to the left, out of the system, and the second term is nothing but the reflected wave, travelling to the right; thus, we can identifty $R(\omega)$ as the *reflectivity* associated with the BC at $x=-L$. Note that the waveform (3.3) is only a valid solution to Eq. (3.1) if $V(x\sim -L)=0$. In the perturbative formalism that we will employ this will not be a problem - our results will be completely general (which is not the case in previous approaches [12]).

Furthermore, if we do not wish for external influence on the system, the reflectivity should also obey

$$|R(\omega)|\leq 1\,, \tag{3.4}$$

otherwise, the reflected wave has a larger amplitude than the outgoing wave, i.e. there is an external input at the left. The condition above is however violated for some well-known systems, such as Kerr black holes, which are known to display superradiance [31].

We note that this condition is *not* a necessary assumption for our approach, even though it is needed if we want *decaying* echoes.

The reflection coefficient $R(\omega)$ is completely specified by the BC at $x = -L$. We can point out three familiar cases. For a purely outgoing wave to the left, we simply have $R(\omega) = 0$. For a Dirichlet BC, imposing $\Psi(t, -L) = 0$ on Eq. (3.3), we have $R(\omega) = -e^{i\omega 2L}$, whereas for a Neumann BC ($\partial_x \Psi(t, -L) = 0$) we get $R(\omega) = e^{i\omega 2L}$. Both of the latter two are conservative boundary conditions since they satisfy $|R(\omega)| = 1$.

Alternatively, $R(\omega)$ can be specified and the BC at $x = -L$ becomes automatically imposed. For instance, dissipation can be introduced by generalizing the latter reflectivities to

$$R(\omega) = -re^{i\omega 2L}\,, \tag{3.5}$$

with $r \in [-1, 1]$ and $|R(\omega)| = |r| \leq 1$. The BC at $x = -L$ turns out to be $\Psi(t, -L) \propto (1 - r)e^{i\omega(L-t)}$ and $\partial_x \Psi(t, -L) \propto -i\omega(1 + r)e^{i\omega(L-t)}$.

3.2 The Dyson series solution of the Lippman-Schwinger equation

To solve Eq. (3.1) we employ the Laplace transform [15]

$$\tilde{\Psi}(\omega, x) = \int_0^{\infty} \Psi(t, x)e^{i\omega t}\, dt, \tag{3.6}$$

where the usual Laplace coordinate is related to the frequency through $s = -i\omega$. In this case, if $\Psi(t \to \infty) \sim e^{\alpha t}$ then $\tilde{\Psi}$ only converges for $\Im\omega > \alpha$.

The time-dependent solution is then the inverse of this transform,

$$\Psi(t, x) = \frac{1}{2\pi} \int_{-\infty+i\beta}^{+\infty+i\beta} \tilde{\Psi}(\omega, x)e^{-i\omega t}\, d\omega\,, \tag{3.7}$$

where β assumes any value $\beta > \alpha$ to ensure the integrand is always convergent along the path of integration.

With these definitions, Eq. (3.1) is reduced to the non-homogeneous ODE

$$\frac{d^2\tilde{\Psi}}{dx^2} + \big(\omega^2 - V(x)\big)\tilde{\Psi} = I(\omega, x)\,, \tag{3.8}$$

with source term

$$I(\omega, x) = i\omega\psi_0(x) - \dot{\psi}_0(x)\,, \tag{3.9}$$

and $\psi_0(x) = \Psi(0, x)$ and $\dot{\psi}_0(x) = \partial_t \Psi(0, x)$ encorporating the initial data at $t = 0$.

Now, instead of pursuing the usual Green's function approach, we shall take a perturbative framework.

The ODE (3.8), and BCs, can be jointly expressed in the integral form, called the Lippman-Schwinger equation,

$$\tilde{\Psi}(\omega, x) = \tilde{\Psi}_0(\omega, x) + \int_{-L}^{\infty} g(x, x')\, V(x')\tilde{\Psi}(\omega, x')\, dx'\,, \tag{3.10}$$

where

$$g(x, x') = \frac{e^{i\omega|x-x'|} + R(\omega)\, e^{i\omega(x+x')}}{2i\omega}\,, \tag{3.11}$$

is the Green's function of the free wave operator $d^2/dx^2 + \omega^2$ with BCs (3.2) and (3.3), and

$$\tilde{\Psi}_0(\omega, x) = \int_{-L}^{\infty} g(x, x')\, I(\omega, x')\, dx'\,, \tag{3.12}$$

is the free-wave amplitude.

The formal solution of Eq. (3.10) is the Dyson series

$$\tilde{\Psi}(\omega, x) = \sum_{k=1}^{\infty} \int_{-L}^{\infty} g(x, x_1) \cdots g(x_{k-1}, x_k) V(x_1) \cdots V(x_{k-1}) I(\omega, x_k) dx_1 \cdots dx_k\,, \tag{3.13}$$

which effectively works as an expansion in powers of V/ω^2 (and thus is expected to converge for high frequencies ω) since $g \propto 1/\omega$ and $dx \sim 1/\omega$.

Note that if we were to expand each term of the series with explicit use of (3.11) we would get a panoply of powers of $R(\omega)$. Now, we may ask, is it possible to reorganize (3.13) and express it as a series in powers of $R(\omega)$? This is the main task of this work.

3.3 Resummation of the Dyson series and echoing structure

We start by dividing the Green's function (3.11) into $g = g_o + R\, g_r$, with

$$g_o(x, x') = \frac{e^{i\omega|x-x'|}}{2i\omega}\,, \tag{3.14}$$

the open system Green's function, and

$$g_r(x, x') = \frac{e^{i\omega(x+x')}}{2i\omega}\,, \tag{3.15}$$

the "reflection" Green's function.

Then, we can write (3.10) as

$$\begin{aligned}
\tilde{\Psi}(\omega, x) = &\int_{-L}^{\infty} g_o(x, x')\, I(\omega, x')\, dx' \\
&+R(\omega) \int_{-L}^{\infty} g_r(x, x')\, I(\omega, x')\, dx' \\
&+ \int_{-L}^{\infty} g(x, x')\, V(x')\tilde{\Psi}(\omega, x')\, dx'\,.
\end{aligned} \tag{3.16}$$

Now, exactly as the Dyson series was first obtained, we replace the $\tilde{\Psi}(\omega, x')$ in the third integral with the entirety of the rhs of Eq. (3.16), now evaluated at x'. Collecting powers of $R(\omega)$ yields

$$
\begin{aligned}
\tilde{\Psi} = & \int g_o I + \int\int g_o V g_o I \\
& + R\left[\int g_r I + \int\int (g_r V g_o + g_o V g_r) I\right] \\
& + R^2 \int\int g_r V g_r I \\
& + \int\int g\, V g\, V \tilde{\Psi}\,,
\end{aligned}
\tag{3.17}
$$

where, for better clarity, we chose not to write the functions' arguments.

If we repeat the process one more time - by replacing Eq. (3.16) with $\tilde{\Psi}$ in the last integration in (3.17) - we get

$$
\begin{aligned}
\tilde{\Psi} = & \int g_o I + \int\int g_o V g_o I + \int\int\int g_o V g_o V g_o I \\
& + R\left[\int g_r I + \int\int (g_r V g_o + g_o V g_r) I + \int\int\int (g_o V g_o V g_r + g_o V g_r V g_o + g_r V g_o V g_o) I\right] \\
& + R^2 \left[\int\int g_r V g_r I + \int\int\int (g_o V g_r V g_r + g_r V g_r V g_o + g_r V g_o V g_r) I\right] \\
& + R^3 \int\int\int g_r V g_r V g_r I \\
& + \int\int\int g\, V g\, V g\, V \tilde{\Psi}\,,
\end{aligned}
\tag{3.18}
$$

and a pattern starts to emerge. The first line does not contain any g_r, the second line contains one g_r arranged in all possible distinct ways with the g_o's, the third line contains two g_r's also arranged in all possible ways, and so on and so forth. If we continue this process we end up with a geometric-like series in powers of the reflectivity R,

$$
\tilde{\Psi}(\omega, x) = \tilde{\Psi}_o(\omega, x) + \sum_{n=1}^{\infty} \tilde{\Psi}_n(\omega, x)\,,
\tag{3.19}
$$

with each term a Dyson series itself:

$$
\tilde{\Psi}_o(\omega, x) = \sum_{k=1}^{\infty} \int_{-L}^{\infty} g_o(x, x_1) \cdots g_o(x_{k-1}, x_k) V(x_1) \cdots V(x_{k-1}) I(\omega, x_k) dx_1 \cdots dx_k\,,
\tag{3.20}
$$

the series stemming from the first line of (3.18), and the reflectivity terms, which can be re-arranged as,

$$
\begin{aligned}
\tilde{\Psi}_n(\omega, x) = R^n(\omega) \sum_{k=n}^{\infty} \int_{-L}^{+\infty} \sum_{\{k,n\}} & g_r(x, x_1) \cdots g_r(x_{n-1}, x_n)\, g_o(x_n, x_{n+1}) \cdots g_o(x_{k-1}, x_k) \\
& V(x_1) \cdots V(x_{k-1}) I(\omega, x_k) dx_1 \cdots dx_k\,,
\end{aligned}
\tag{3.21}
$$

where $\sum_{\{k,n\}}$ is a sum on all possible distinct ways of ordering n g_r's in k spots, resulting in a total of $\binom{k}{n}$

terms. For example,

$$\sum_{\{3,2\}} g_r(x,x_1)g_r(x_1,x_2)g_o(x_2,x_3)V(x_1)V(x_2)I(\omega,x_3) =$$
$$g_r(x,x_1)g_r(x_1,x_2)g_o(x_2,x_3)V(x_1)V(x_2)I(\omega,x_3)$$
$$+ g_r(x,x_1)g_o(x_1,x_2)g_r(x_2,x_3)V(x_1)V(x_2)I(\omega,x_3)$$
$$+ g_o(x,x_1)g_r(x_1,x_2)g_r(x_2,x_3)V(x_1)V(x_2)I(\omega,x_3)\,, \tag{3.22}$$

we see that the functions' arguments remain in the same relative position and only the g_r's and g_o's interchange.

There is no doubt we have increased the mathematical complexity of the problem. Nonetheless, Eq. (3.21) has special significance: it is the frequency amplitude of the n-th *echo* of the initial perturbation. There is no proper way to show this since there is no rigorous mathematical definition of an echo. However, with the following discussion and further application of this formalism to the Dirac delta potential in Chapter 4, we hope to provide enough justification.

If $R = 0$ then $\tilde{\Psi} = \tilde{\Psi}_o$, the open system waveform, where only g_o participates. Conversely, when we do not have a perfectly permeable boundary ($R \neq 0$), we get an additional infinite number of Dyson series, as stated in Eq. (3.19). These $\tilde{\Psi}_n$ terms are expected to give a smaller contribution to $\tilde{\Psi}$ as n increases, in other words, a *decay* of successive echoes should be observed. This is mainly due to two features in (3.21).

- First, when $|R(\omega)| < 1$, $R^n(\omega)$ is obviously an attenuation factor with a larger impact at large n. It indicates n partial reflections at the boundary, as effectively done by the n-th echo. It should also be noted that echoes have the distinctive feature of being spaced by the same distance for any pair of successive echoes. The fact that $\tilde{\Psi}_{(n+1)}$ has an additional factor of $R(\omega)$ than $\tilde{\Psi}_{(n)}$, hence an, independent of n, phase difference of $\arg[R(\omega)]$, indicates this.

- More subtle is the fact that the Dyson series starts at $k = n$. Since g_o and g_r are of the same order of magnitude, it is natural to expect that the series starting ahead (with less terms) has a smaller magnitude and contributes less to $\tilde{\Psi}$ than the ones preceding them. The additional term that $\tilde{\Psi}_n$ possesses when compared to $\tilde{\Psi}_{n+1}$, and hence can be used to evaluate their amplitude difference, is given by

$$\Delta_n(\omega,x) = R^n(\omega)\int_{-L}^{\infty} g_r(x,x_1)\cdots g_r(x_{n-1},x_n)\,V(x_1)\cdots V(x_{n-1})I(\omega,x_n)dx_1\cdots dx_n\,. \tag{3.23}$$

Furthermore, latter echoes are seen to vibrate less than the first echoes. As we mentioned before, since the Dyson series is basically an expansion on powers of V/ω^2, $\tilde{\Psi}_n$ skips the high frequency contribution to the series until $k = n$ since the series commences in this term. The intuitive interpreation comes from high frequency signals tunneling through the potential barrier more easily than lower frequency signals, which is the reason why high frequency behaviour predominates in the earlier echoes and is verified in expression (3.21).

3.4 Inversion into the time domain

Finally, let us make use of the inverse Laplace transform (3.7) to obtain the time-dependent solution of wave equation (3.1). We start with the open system perturbation $\tilde{\Psi}_o$, given by Eq. (3.20). Here, the ω dependent terms are the Green's functions g_o, which have a pole at $\omega = 0$ (Eq. (3.14)), and the source term I which does not have any pole (Eq. (3.9)). Thus, to keep the integrand convergent we should integrate above $\omega = 0$. The frequency integral of the k-th term of (3.20) is

$$\frac{1}{2\pi i}\int_{-\infty+i}^{+\infty+i} \frac{e^{i\omega(|x-x_1|+\cdots+|x_{k-1}-x_k|-t)}}{\omega^k} I(\omega, x_k)\, d\omega\,, \tag{3.24}$$

where we have chosen $\beta = 1\,(>0)$, in Eq. (3.7). The integrand is non-analytic except when $k = 1$, due to the term $i\omega\psi_0(x)$ in $I(\omega, x)$, that cancels the ω in the denominator. For this term, we have

$$\frac{1}{2\pi}\int_{-\infty+i}^{+\infty+i} e^{i\omega(|x-x_1|-t)}\, d\omega = \delta(|x-x_1|-t)\,, \tag{3.25}$$

whereas for the contribution $-\dot{\psi}_0(x)$ in $I(\omega, x)$, we only have to integrate a simple pole at $\omega = 0$ to get

$$-\frac{1}{2\pi i}\int_{-\infty+i}^{+\infty+i} \frac{e^{i\omega(|x-x_1|-t)}}{\omega}\, d\omega = \Theta(t-|x-x_1|)\,, \tag{3.26}$$

which vanishes for $t < |x - x_1|$: The initial signal $\dot{\psi}_0(x_1)$ did not have enough time to travel to the point of observation x, i.e. these points are *causally* disconnected.

Integration of $\psi_0(x_1)$ and $\dot{\psi}_0(x_1)$ with (3.25) and (3.26), respectively, yields the first term of $\Psi_o(t, x)$, associated with free propagation of the initial waveform,

$$\Psi_i(t,x) = \frac{1}{2}\left[\psi_0(x-t) + \psi_0(x+t) + \int_{x-t}^{x+t} \dot{\psi}_0(x')\, dx'\right]. \tag{3.27}$$

If both $R(\omega)$ and $V(x)$ vanish, this corresponds to the exact complete solution, $\Psi_i(t, x) = \Psi(t, x)$. The equation above reveals that the initial waveform separates in two halves, propagating in opposite directions, as we would expect in a plucked infinite string.

For $k \neq 1$, we start by defining

$$s_k := |x-x_1| + \cdots + |x_k - x_{k+1}| - t\,, \tag{3.28}$$

interpeted as the causal distance, involving k interaction points besides the point of observation x and the source point x_{k+1}, for an elapsed time t.

With this definition the argument of the exponential in (3.24) is simply $i\omega s_{k-1}$. This integration, for $k \neq 1$ yields

$$\frac{\Theta(-s_{k-1})}{(k-1)!}\,\frac{\partial^{k-1}}{\partial\omega^{k-1}}\left[e^{i\omega s_{k-1}} I(\omega, x_k)\right]_{\omega=0}. \tag{3.29}$$

If $I(\omega, x_k)$ was independent of ω, the term in brackets would only correspond to the the derivatives of the phase factor, $(is_{k-1})^{k-1} I(x_k)$. But since I has the linear form (3.9), we can write the term inside brackets as $(is_{k-1})^{k-1} I(-i\frac{k-1}{s_{k-1}}, x_k)$.

Putting everything together yields a Taylor-like expansion,

$$\Psi_o(t,x) = \Psi_i(t,x) - \frac{1}{2}\sum_{k=1}^{\infty}\frac{1}{k!}\int_{-L}^{\infty}\Big(\frac{s_k}{2}\Big)^k I\Big(-\frac{ik}{s_k}, x_{k+1}\Big)V(x_1)\cdots V(x_k)\,\Theta(-s_k)\,dx_1\cdots dx_{k+1}\,. \tag{3.30}$$

Laplace inversion of Eq. (3.21) follows the same lines. Instead of s_k, it is useful to define

$$\sigma_{n,k} := (x-x_1)+\cdots+(x_{n-1}+x_n)+|x_n-x_{n+1}|+\cdots+|x_{k-1}-x_k|-t\,, \tag{3.31}$$

so that the frequency integral, corresponding to inversion of the k-th term of (3.21) through (3.7), can be written as

$$\frac{1}{2\pi i}\int_{-\infty+i}^{+\infty+i}\frac{e^{i\omega\sigma_{n,k}}}{\omega^k}R^n(\omega)\,I(\omega,x_k)\,d\omega\,, \tag{3.32}$$

where we replaced the Green's functions g_o and g_r by their explicit forms (3.14) and (3.15), respectively.

Unfortunately now we cannot go further unless we know $R(\omega)$ in detail: its poles and divergent behaviour at $\pm i\infty$, which allows us to specify the choice of contour.

Thus, for completeness, we present below the calculation for R given by Eq. (3.5):

$$\Psi_n(t,x) = \delta_{n,1}\Psi_r(t,x) - \frac{(-r)^n}{2}\sum_{k=n}^{\infty}\int_{-L}^{\infty}\sum_{\{k,n\}}\frac{(\sigma_{n,k}+2Ln)^{k-1}}{2^{k-1}(k-1)!}I\Big(-\frac{i(k-1)}{\sigma_{n,k}+2Ln}, x_k\Big)V(x_1)\cdots V(x_{k-1})$$
$$\Theta(-\sigma_{n,k}-2Ln)\,dx_1\cdots dx_k\,, \tag{3.33}$$

with

$$\Psi_r(t,x) = -\frac{r}{2}\psi_0(t-x-2L) \tag{3.34}$$

corresponding to the reflected initial waveform (if $\dot\psi_0 = 0$), present only in the first echo (due to the Kronecker delta $\delta_{n,1}$).

The more attentive reader may realize that the inversion into the time domain is only practically performed if the explicit form of $R(\omega)$ is known. For instance, this is not the case for a wormhole system, where R stands for the reflectivity of the Schwarzshcild potential, which can only be extracted numerically. Thus, one may ask if it is also possible to express the reflectivity of a generic potential as a perturbative series in $V(x)$. The answer is a definite yes.

3.5 Reflectivity series

If a wave is sent from $+\infty$ ($e^{-i\omega x}$), the reflectivity will be the factor of the reflected wave, $R(\omega)e^{i\omega x}$. The source $I(\omega,x)$ that corresponds to $\tilde\Psi_0 = e^{-i\omega x}$ can be inspected from (3.12), with $g = g_o$ (we are trying to extract the reflectivity, so it is only natural to consider purely outgoing BCs at both sides), and formally reads as

$$I(\omega,x) = 2i\omega\lim_{l\to\infty}\delta(x-l)\,e^{-i\omega l} \tag{3.35}$$

which non surprisingly corresponds to a source pulse located at $x \to \infty$ (the factor of $e^{-i\omega l}$ takes care of the phase difference coming from ∞).

Now, with this source term, the solution given by the Dyson series (3.20) at $x \to \infty$ is straightforwardly seen to have the form $\tilde{\Psi}(\omega, x \to \infty) = e^{-i\omega x} + R(\omega)\, e^{i\omega x}$, with

$$R(\omega) = \sum_{k=1}^{\infty} \frac{1}{(2i\omega)^k} \int_{-\infty}^{\infty} e^{i\omega(-x_1+|x_1-x_2|+\cdots+|x_{k-1}-x_k|-x_k)} V(x_1)\cdots V(x_k)\, dx_1 \cdots dx_k\,, \tag{3.36}$$

the reflection coefficient expressed in terms of the potential, as promised.

The above expression can also be used to compute the system's QNMs, which are the poles of $R(\omega)$. In fact, there is an ongoing discussion within the community regarding whether the QNMs of the system with purely outgoing BCs at both sides (as in the above case) coincide with the ones where a mirror is introduced, replacing the outgoing BC at one side with some other different BC like the one we specified in (3.3).

Now, the mirror + potential system's QNMs should also be the poles of its ”reflectivity”. This concept, however, is not defined in the case both BCs are not purely outgoing, that is, if the system is only partially open. We cannot simply take the initial wave as $\tilde{\Psi}_0 = e^{-i\omega x}$ but instead we should consider

$$\tilde{\Psi}_0 = e^{-i\omega x} + R(\omega) e^{i\omega x}\,, \tag{3.37}$$

where $R(\omega)$ is NOT the reflectivity of the system but the reflectivity associated with the non trivial BC at some $x = -L$. This is the correct form for $\tilde{\Psi}_0$ since, by Eq. (3.10), it should also be the complete solution of the system when there is no potential barrier and additionally reduce to $e^{-i\omega x}$ when the mirror vanishes, that is, a free travelling to the left plane wave.

The reader may find comfort in this definition by noting that $\tilde{\Psi}_0$ computed through Eq. (3.12) with I given by Eq. (3.35) does indeed recover expression (3.37).

Naturally, the system's reflectivity can only correspond to the factor multiplying the outgoing wave at $+\infty$, $\mathcal{R}(\omega)\, e^{i\omega x}$. With the source term (3.35) and g given by Eq. (3.11), we just need to evaluate expression (3.13) at $x \to \infty$ to identify

$$\mathcal{R}(\omega) = R(\omega) + \frac{1}{2i\omega} \sum_{k=1}^{\infty} \int_{-L}^{\infty} (e^{-i\omega x_1} + Re^{i\omega x_1}) g(x_1,x_2) \cdots g(x_{k-1}, x_k)(e^{-i\omega x_k} + Re^{i\omega x_k})$$
$$V(x_1)\cdots V(x_k)\, dx_1 \cdots dx_k\,, \tag{3.38}$$

which reduces to $\mathcal{R} = R$ if the potential vanishes, and to Eq. (3.36) if $R \to 0$, as expected. We emphasize that $R(\omega)$ in the above expression corresponds to the reflectivity associated with the non-trivial BC at $x = -L$ whereas, in (3.36), it is the reflectivity of the potential barrier. We use the same letter for both since the mirror at $x = -L$ can be either due to a non-outgoing boundary condition at this point, or a potential barrier, in this case computable through Eq. (3.36).

We can see that Eq. (3.38) does not diverge where Eq. (3.36) diverges, for arbitrary potential. In other words, the mirror+potential system and the completely open potential system do not share the same spectrum of quasinormal modes.

In the next chapter, we apply all this apparatus to a specific $V(x)$, the Dirac delta potential.

Chapter 4

Echoes of a Membrane-Mirror cavity

A Dirac delta potential located at $x = 0$,

$$V(x) = 2V_0\,\delta(x)\,, \tag{4.1}$$

with $V_0 > 0$, and a mirror with reflectivity $R(\omega)$ placed at $x = -L$, constitute a lossy cavity in the region $x \in]-L, 0[$, which we call a Membrane-Mirror cavity.

What follows is application of the formalism of Chapter 3 with potential (4.1).

4.1 Open system solution: Ψ_o

Instead of employing straight ahead the formula for the time-dependent open system solution, Eq. (3.30), it is interesting to first compute the frequency amplitude from Eq. (3.20) and then Laplace invert it. The $k = 1$ term corresponds to the free propagating initial waveform, $\tilde{\Psi}_i(\omega, x)$ given by the Laplace inversion of Eq. (3.27). For $k > 1$, the $k-1$ delta functions collapse all the integrals except the integration in x_k to give

$$\tilde{\Psi}_o(\omega,x) = \tilde{\Psi}_i(\omega, x) + \sum_{k=2}^{\infty} \int_{-L}^{\infty} \frac{e^{i\omega(|x|+|x_k|)}}{(2i\omega)^k} (2V_0)^{k-1} I(\omega, x_k)\, dx_k\,, \tag{4.2}$$

which, in fact, is a k-independent integral: Relabeling $x_k \to x'$ and treating the sum as a geometric series, simplifies the above to

$$\tilde{\Psi}_o(\omega, x) = \tilde{\Psi}_i(\omega, x) + \int_{-L}^{\infty} \frac{e^{i\omega(|x|+|x'|)}}{2i\omega} R_\delta(\omega)\, I(\omega, x')\, dx', \tag{4.3}$$

where

$$R_\delta(\omega) = \sum_{k=1}^{\infty} \left(\frac{V_0}{i\omega}\right)^k = -\frac{V_0}{V_0 - i\omega} \tag{4.4}$$

is the reflection coefficient of the Dirac delta potential (4.1), which could be directly computed from Eq. (3.36) and diverges at the (single) QNM

$$\omega = -iV_0\,. \tag{4.5}$$

With $\tilde{\Psi}_o$ in hand we just have to apply Eq. (3.7) to get the time-dependent solution:

$$\Psi_o(t,x) = \Psi_i(t,x) - C_0(t-|x|) + C_{V_0}(t-|x|)\, e^{-V_0(t-|x|)}\,, \tag{4.6}$$

with QNM excitation coefficient given by

$$C_{V_0}(t) = -\frac{1}{2}\,\Theta(t)\int_{-t}^{t} e^{V_0|x|}\, I(-iV_0,x)\,dx\,, \tag{4.7}$$

and $\Psi_i(t,x)$ given by (3.27).

Direct application of Eq. (3.30) would even be more straightforward: Instead of a geometric series, the infinite series that factors out is the Taylor expansion of $e^{V_0(|x|+|x'|-t)}$.

Before we advance, we should point out the following. When there are no interactions, $V_0 = 0$, the two latter terms of (4.6) cancel each other and, as expected, $\Psi_o(t,x) = \Psi_i(t,x)$. More interestingly, unlike conservative systems, the QNM excitation coefficient C_{V_0} is not a constant. Thus, in which conditions does $\Psi_o(t,x)$ decay with the QNM behaviour? We expect this to happen when $I(\omega,x)$ is sufficiently localized in space, which should occur in more ”physical” sources. Even a decay $I(\omega,x)\sim e^{-a|x|}$, for some $a>0$ gives $\Psi_o(t\to\infty,x)\sim e^{-at}$. For a gaussian source $I(\omega,x)\sim e^{-ax^2}$ it is possible to rewrite the integrand in (4.7) as $\sim e^{-a(x-b)^2}$ with $b=\frac{V_0}{2a}$. Even if the gaussian is disperse (small a), which makes b assume large values, for $t\gg b$ the integrand will contribute little and $C_{V_0}(t)$ is essentially independent of t. In the limit $t\to\infty$, C_{V_0} will just be the real line integral of a gaussian, with convergent and known value and hence $\Psi_o(t\to\infty,x) = C_{V_0}\, e^{-V_0 t}$.

4.2 Echoes: Ψ_n

To obtain $\Psi(t,x)$ we still need to get the echoes $\Psi_n(t,x)$, as specified by Eq. (3.19). Since we have not yet particularized the form of $R(\omega)$, we must start at the frequency amplitude and apply Eq. (3.21) with potential (4.1).

As previously, the delta functions will collapse all integrals in the k-th term of expansion (3.21), except the one in x_k, which results in the sum on all distinct arrangements of the n g_r's in the k spots to assume the form

$$\sum_{\{k,n\}} g_r(x,0)g_r(0,0)\cdots g_r(0,0)g_o(0,0)\cdots g_o(0,0)g_o(0,x_k). \tag{4.8}$$

Since $g_r(0,0) = g_0(0,0)$, according to Eqs. (3.14) and (3.15), a large number of arrangements will turn out to be numerically identical, more specifically, the ones involving interchaning the functions in the 'middle', with argument $(0,0)$. In fact, there are only 4 possible algebraically different outcomes for the pair of functions at both ends of the product, which make the above simplify to

$$g_r(x,0)g_r(0,x_k)\binom{k-2}{n-2}+g_o(x,0)g_o(0,x_k)\binom{k-2}{n}+\left[g_o(x,0)g_r(0,x_k)+g_r(x,0)g_o(0,x_k)\right]\binom{k-2}{n-1}. \tag{4.9}$$

To get the first term, for instance, we have a couple of g_r's at the ends, leaving $k-2$ spots for the remaining $n-2$ g_r's. The others follow the same reasoning. Even if not directly apparent, we are dealing with a total number of $\binom{k}{n}$ terms, as pointed out after Eq. (3.21), since

$$\binom{k-2}{n-2}+2\binom{k-2}{n-1}+\binom{k-2}{n}=\binom{k}{n}. \tag{4.10}$$

Now, similarly to what happened in Eq. (4.2), renaming $x_k \to x'$ will make the integral (3.21) independent of k and a geometric-like series factors out for every term in Eq. (4.9). For $g_r(x,0)g_r(0,x')$, for example, what factors out is the power of the delta reflectivity

$$\sum_{k=n}^{\infty}\binom{k-2}{n-2}\left(\frac{V_0}{i\omega}\right)^{k-1}=\left[R_\delta(\omega)\right]^{n-1}, \tag{4.11}$$

with R_δ given by Eq.(4.4), where the following identity for the power of a geometric series was employed,

$$\sum_{k=n}^{\infty}\binom{k-1}{n-1}r^k=\left[\sum_{k=1}^{\infty}r^k\right]^n. \tag{4.12}$$

Using the above for the remaining terms yields

$$\tilde{\Psi}_n(\omega,x)=\int_{-L}^{\infty}\Big[R_\delta^{n-1}(\omega)e^{i\omega(x+x')}+R_\delta^{n+1}(\omega)e^{i\omega(|x|+|x'|)}+R_\delta^{n}(\omega)\big(e^{i\omega(x+|x'|)}+e^{i\omega(|x|+x')}\big)\Big]R^n(\omega)\frac{I(\omega,x')}{2i\omega}dx'. \tag{4.13}$$

This panoply of terms bears an enlightening interpretation. The first one, with the product $R_\delta^{n-1}R^n$, corresponds to a wave sent left, towards the mirror, and also received from the mirror, travelling to the right. Take the second echo, $n=2$, for example. It first reflects at the mirror, then at the delta, and again at the mirror, picking up a factor $R_\delta R^2$.

The second one, with $R_\delta^{n+1}R^n$, is the opposite situation. The wave is sent to the right, towards the delta, and then also received from the delta, but travelling to the left. This situation can only happen for $x\in[-L,0]$, when the observer is inside the cavity.

The same is verified for the last two terms, with $R_\delta^n R^n$. Here, one of two situations happen. The wave is first sent into the mirror and then received from the delta, or sent into the delta and then received from the mirror, reflecting either way an equal number of times at the delta and at the mirror.

The echoes' amplitude $\tilde{\Psi}_n$ is similar, in form, to $\tilde{\Psi}_0$. Besides the presence of R^n, the difference lies in the order of the pole of the QNM (4.5), due to the powers of R_δ. Inversion will result in derivatives of the integrand, evaluated at the QNM. The echoes, besides vibrating and decaying with the delta QNM, have a slightly different behaviour. For trivial I, for instance, the derivative will only act on the phase factor

$\sim e^{i\omega(x-t)}$ assigning, additionally, a *polynomial* behaviour to the echoes' waveform.

To proceed with inversion, with the use of Eq. (3.7), we consider $R(\omega)$ given by Eq. (3.5), to get

$$\Psi_n(t,x) = \delta_{n,1}\frac{r}{2}\left[-\psi_0(t-x-2L)+\int_{-L}^{t-x-2L} I(0,x')dx'\right]$$
$$-\frac{(-r)^n}{2}\Big(E_n(V_0;t-|x|-2Ln)+E_{n-1}(V_0;t-x-2Ln)-E_n(0;t-|x|-2Ln)-E_{n-1}(0;t-x-2Ln)\Big) \tag{4.14}$$

with

$$E_n(V_0;t) = \Theta(t)\frac{V_0^{n+1}}{n!}\frac{\partial^n}{\partial V_0^n}\int_{-\min(t,L)}^{t} e^{V_0(|x|-t)}\frac{I(-iV_0,x)}{V_0}dx$$
$$+\Theta(t+L)(1-\delta_{n,0})\frac{V_0^n}{(n-1)!}\frac{\partial^{n-1}}{\partial V_0^{n-1}}\int_{-L}^{t} e^{V_0(x-t)}\frac{I(-iV_0,x)}{V_0}dx. \tag{4.15}$$

A few comments must be made. Interaction of the source with the delta is being accounted in the first integral of Eq. (4.15) whereas reflection at the mirror is taken into account in the second integral, hence the Θ functions ensuring that there is enough time for the source to reach the membrane and the mirror, respectively.

The factor $(1-\delta_{n,0})$ vanishes for $n=0$ and is 1 otherwise. It is easy to see that it only vanishes for Ψ_1, the first echo, which instead possesses the term on the first line of Eq. (4.14), corresponding to the reflection at $x=-L$ of the left-travelling intial waveform. This is the only surviving term in case $V_0 \to 0$, when there is no cavity.

It is relevant to note that the integrals themselves do not depend on n, apart from the integration limits. The difference between echoes mostly lies in the order of the derivative on V_0.

Figure 1 below shows a "time-lapse" of the complete waveform given by the sum of the open-system solution, Eq. (4.6), with the first 3 echoes, described by Eq. (4.14), with a gaussian static initial condition

$$\psi_0(x) = e^{-(x-10)^2}\,, \quad \dot{\psi}_0(x) = 0\,. \tag{4.16}$$

and parameters

$$V_0 = 1\,, \quad L = 10\,, \quad r = 1 \text{ (Dirichlet BC)}. \tag{4.17}$$

A complete sequence of events up until the 8-th echo can be seen in video format at: `https://youtu.be/XfJNwuwbvnA`.

4.3 QNMs

To illustrate the discussion at the end of Chapter 3, let us compute the membrane-mirror system's reflectivity. Equation (3.38) with potential (4.1) yields

$$\mathcal{R}_\delta = R + (1+R)\sum_{k=1}^{\infty}\left[(1+R)\frac{V_0}{i\omega}\right]^k, \tag{4.18}$$

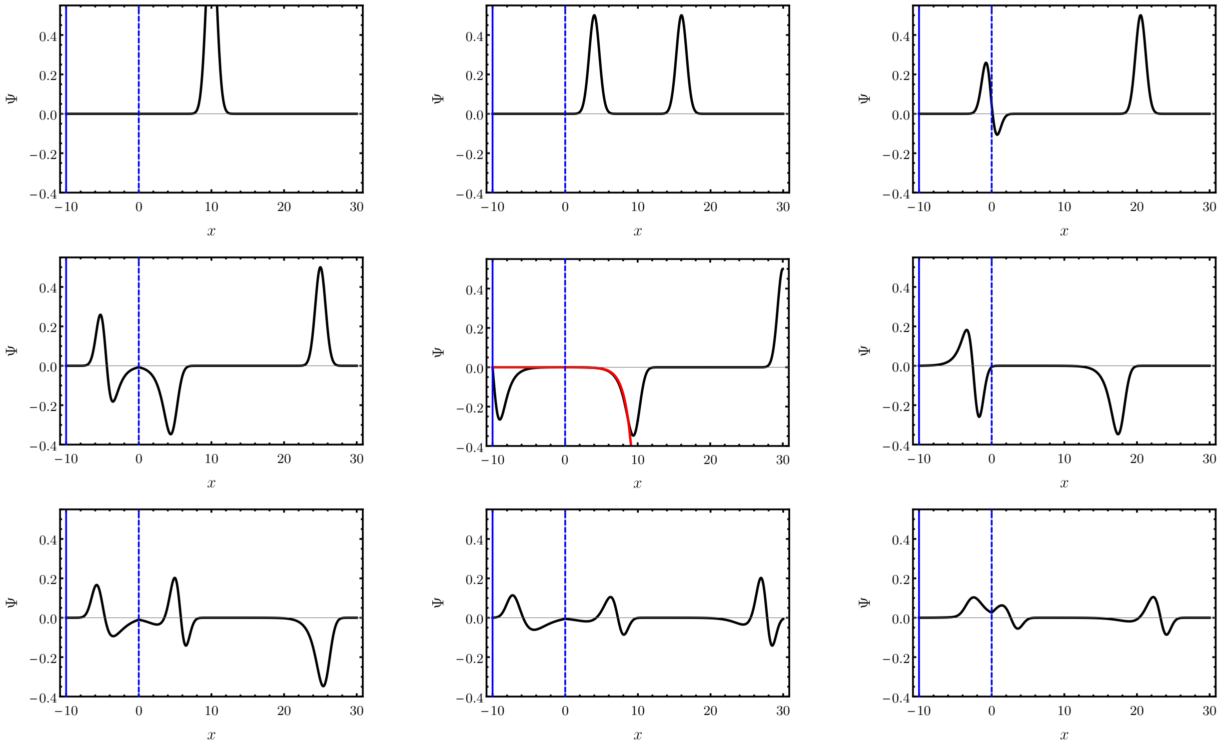

Figure 4.1: Snapshots of the scalar profile at $t = 0, 6, 10.5, 16, 20, 28, 36, 58, 74$ (top to bottom, left to right) in the presence of a delta-like potential at $x = 0$ and a mirror at $x = -10$. The initial profile (4.16) quickly gives way to two pulses traveling in opposite directions at $t = 6$, as described by Eq. (3.27); the left propagating pulse interacts with the (delta) potential at $t = 10.5$ and gives rise to a transmitted pulse and a reflected one ($t = 16$). The reflected pulse eventually reaches the boundary, at $t = 20$, and will cross the potential at around $t = 36$ giving rise to the first echo. The wave confined to the cavity (mirror+potential) will produce all subsequent echoes. At $t = 58$, after $2L = 20$ time units the second echo emerges out of the cavity and at $t = 74$ a third echo is about to be produced. These snapshots were obtained by adding three “echoes,” and coincides up to numerical error, with the waveform obtained via numerical evolution of the initial data. In the central panel, the red line shows $-e^{V_0(x-10)}$, confirming that the initial decay is described by the QNMs (4.5) of the pure delta function (no mirror).

which simplifies to

$$\mathcal{R}_\delta = \frac{R_\delta + R + 2R_\delta R}{1 - R_\delta R}\,, \tag{4.19}$$

when the geometric series identity and definition of R_δ, Eq. (4.4), are employed.

It is easy to check that $\mathcal{R}_\delta \to R_\delta$ if $R \to 0$ and vice-versa, if $R_\delta \to 0$ then $\mathcal{R}_\delta \to R$. In fact, we can see that $\mathcal{R}_\delta$ is a symmetric function of (R, R_δ). Moreover, if $R = -1$, corresponding to a perfectly reflecting mirror, then we should expect everything to be reflected back, independently of the potential. In this limit we also see that $\mathcal{R}_\delta = -1$.

More interestingly, at the QNM (4.5) we have that $R_\delta \to \infty$ and the dependence on R_δ cancels to give $\mathcal{R}_\delta = -\frac{1+2R}{R}$, which is finite for a non-trivially vanishing R. Thus, $\omega = -iV_0$ is NOT a QNM of the mirror+delta system. The QNMs are instead implicitly given by the poles of $\mathcal{R}_\delta$ which must satisfy

$$R(\omega_n)R_\delta(\omega_n) = 1\,. \tag{4.20}$$

Fig.4.2 plots the frequencies that respect the above, for R given by Eq. (3.5), with $r = 1$ (Dirichlet BC

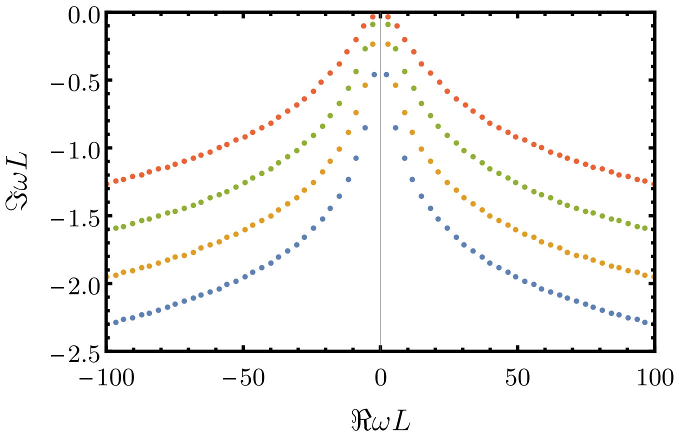

Figure 4.2: QNM frequencies of the membrane-mirror system for different values of $V_0 L = 1, 2, 4, 8$ from bottom (blue) to top (red), respectively.

at $x = -L$), which are well-approximated by the expression

$$\omega_n = \frac{n\pi}{L} - \frac{1}{2L}\arctan\frac{n\pi}{LV_0} - \frac{i}{4L}\log\left(1 + \frac{n^2\pi^2}{L^2V_0^2}\right). \tag{4.21}$$

Not surprisingly, the imaginary part grows in magnitude with $|n|$. This implies that, at sufficiently long times, the perturbation will decay with the fundamental mode $\omega_{\pm 1}$ (Fig. 3), even if the initial perturbation decays according to the pure-delta QNM (4.5) (and as we show in Figure 1). We believe

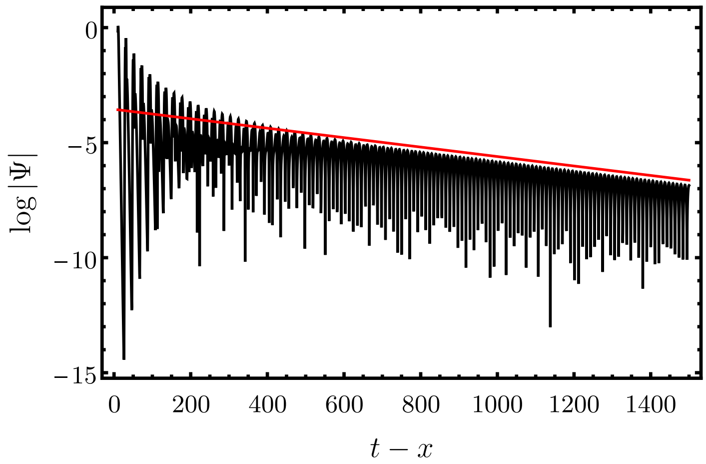

Figure 4.3: Time evolution of the waveform using initial conditions (4.16) and parameters (4.17). The plot shows the decay with the fundamental mode of the system (with mirror on the left), $\Im\omega_{\pm 1} \approx -0.00205$ (in red), for large t. The early echoes decay in a way that is governed by the QNMs of the *pure* delta. The high-frequency component is filtered out and progressively the signal is described by the modes of the composite system at late times, as it should.

that this is the most convincing demonstration to date that the late-time decay is indeed governed by the QNMs of the composite system.

Chapter 5

Conclusions

5.1 Results and achievements

We have shown in Chapter 3 that a proper re-summation of the Dyson series solution of the Lippman-Schwinger equation accounts for the presence of echoes in the waveforms of extremely compact objects (termed “ClePhOs” in the nomenclature of Refs. [32, 33]). We recover previous results, obtained with a completely different approach [12], but our approach, besides being completely general, also provides a few more insights.

The key result Eq.(3.21) besides confirming the lower frequency content, decaying amplitude and constant distance of successive echoes, also explicitly relates the echoes waveform $\Psi_n(t,x)$ with the initial conditions and sources incorporated into $I(\omega,x)$, the potential of the system $V(x)$, and the reflectivity of the wall $R(\omega)$ (the latter two function as the right and left sides of the *lossy* cavity, respectively).

With the hypothetical future discovery of echoes in gravitational wave signals, the echo amplitude $\tilde{\Psi}_n(\omega,x)$ can be extracted up to experimental and numerical error. Together with the knowledge of $V(x)$ and $I(\omega,x)$, this turns Eq. (3.21) into an equation for $R(\omega)$, which encodes the information we currently lack on the quantum structure at the event horizon.

In Chapter 4, we applied this formalism to a Dirac delta potential alongisde a mirror, serving as a simple toy model of a lossy cavity. It is interesting that the delta potential reflectivity arises naturally when the geometric series identity is applied to the already integrated Dyson series, hence revealing how crucial is the delta QNM (being a pole of the reflectivity) in determining the behavior of both the early response and the echoes. Nonetheless, despite having the same damped exponential form, the echoes have a polynomial decay (at early times) that was not explicitly found before. In fact, this is one of the few known explicit solutions of to the wave equation with open BCs, which specifically confirms the hypothesized QNM coefficient dependence on time (contrarily to conservative systems where it is constant).

Albeit not directly related with echoes, both appendices contain a considerable amount of original work done in the past year. The generalized Frobenius method presented in Appendix A allowed us to reduce an originally 5-term recursion relation to the usual 4-term recursion relation obtained at $r \approx r_0$

and further reveal the ingoing BC at the horizon which was kept arbitrary at the start. We also argued that even with a more general expansion there were three terms of the recursion relation that could not be eliminated due to their dependence on n^2. This expansion, first proposed by Leaver in 1985 [22], leads to the said 3-term recursion relation.

Following a lack of a rigorous definition of QNMs and a general equivalence between their intrinsic imaginary negativity and open BCs, we were prompted to establish a first proof of the latter. In section 1 of Appendix B, we showed that purely outgoing BCs in Sturm-Liouville theory turns the wave equation into a non-Hermitian eigenvalue problem for the frequencies ω. In particular, Eq. (B.6) shows that the imaginary part of ω *must be* negative. In the succeeding two sections we show this explicitly by computing the spectrum of a number of toy models involving the Dirac delta and rectangular barrier potentials.

5.2 Future developments and work to be done

Further developments of the resummation formalism introduced in Chapters 3 and 4 should include: an application to other systems (such as a Schwarzschild BH) besides the simple solvable Dirac delta potential; a careful analysis of the convergence properties of Eq. (3.21) (in [34], for instance, the convergence of the usual Born series is shown for localized and rapidly decaying potentials); extension of our methods to more than one spatial dimension given the recent string theoretical arguments of non-spherical symmetry of the quantum corrections to the event horizon; check if superradiant amplification is observed in Eq. (3.21) if $|R(\omega)| > 1$ or if an electric potential is introduced; implementation of the reflectivity series (3.36) and (3.38) to QNM computation; confirm the *polynomial* behaviour of echoes in other systems besides the Dirac delta potential and use this information to echo modelling.

The Frobenius method is the prime approach for obtaining the normal modes of quantum systems, like the energy levels of the Hydrogen atom. Nevertheless, it faces some difficulties when more complicated potentials are introduced or relativistic effects are taken into account. It would be interesting to see if the generalization presented in Appendix A would provide a better answer for more complex systems.

In Appendix B we have seen that in all of the examples the QNM relation can be put into the form $e^{2i\Omega a} R_L(\omega) R_R(\omega) = 1$. Is this general? Can this applied in a smooth procedure as to obtain a general formula for QNM computation? Finally, we see that the modes of the mirror & barrier cavity in subsection B.3.2 have a bounded regime for $n < \frac{\sqrt{V_0}L}{\pi}$, in Eq. (B.45), and a damped regime for $n > \frac{\sqrt{V_0}L}{\pi}$, in Eq. (B.44). Can this effect be studied with the formalism of *phase transitions*? If yes, how does this generalize into other systems?

Bibliography

[1] M.R. Correia and V. Cardoso, *Phys. Rev.* **D97**, 084030 (2018), arXiv:1802.07735.

[2] G.B. Arfken and H.J. Weber, *"Mathematical methods for physicists 6th ed.by George B. Arfken and Hans J. Weber. Published :Amsterdam; Boston : Elsevier, c2005. xii, 1182 p. : ill. ; 25 cm. Includes bibliographical references and index. ISBN :* (2005).

[3] B.P. Abbott *et al.* (Virgo, LIGO Scientific), *Phys. Rev. Lett.* **116**, 241103 (2016), arXiv:1606.04855.

[4] M.D. Schwartz, *"Quantum Field Theory and the Standard Model by Matthew D. Schwartz. Published :USA, Cambridge University Press, c2014. 870 p.; Includes bibliographical references and index. ISBN : 978-1-107-03473-0 Hardback* (2014).

[5] B.P. Abbott *et al.* (The LIGO/Virgo Scientific Collaboration), *Phys. Rev. Lett.* **116**, 061102 (2016), arXiv:1602.03837.

[6] J. Abedi, H. Dykaar, and N. Afshordi, (2016), arXiv:1612.00266.

[7] J. Abedi, H. Dykaar, and N. Afshordi, (2017), arXiv:1701.03485.

[8] G. Ashton, O. Birnholtz, M. Cabero, C. Capano, T. Dent, B. Krishnan, G.D. Meadors, A.B. Nielsen, A. Nitz, and J. Westerweck, (2016), arXiv:1612.05625.

[9] J. Westerweck, A. Nielsen, O. Fischer-Birnholtz, M. Cabero, C. Capano, T. Dent, B. Krishnan, G. Meadors, and A.H. Nitz, (2017), arXiv:1712.09966.

[10] H. Nakano, N. Sago, H. Tagoshi, and T. Tanaka, *PTEP* **2017**, 071E01 (2017), arXiv:1704.07175.

[11] P. Bueno, P.A. Cano, F. Goelen, T. Hertog, and B. Vercnocke, *Phys. Rev.* **D97**, 024040 (2018), arXiv:1711.00391.

[12] Z. Mark, A. Zimmerman, S.M. Du, and Y. Chen, (2017), arXiv:1706.06155.

[13] Y.T. Wang, Z.P. Li, J. Zhang, S.Y. Zhou, and Y.S. Piao, (2018), arXiv:1802.02003.

[14] D.J. Griffiths, *Introduction to quantum mechanics*, 2nd ed. (Pearson / Prentice Hall, 2005).

[15] E. Berti, V. Cardoso, and A.O. Starinets, *Class. Quantum Grav.* **26**, 163001 (2009), arXiv:0905.2975.

[16] T. Regge and J.A. Wheeler, *Phys. Rev.* **108**, 1063 (1957).

[17] F. Zerilli, *Phys. Rev.* **D2**, 2141 (1970).

[18] C.V. Vishveshwara, *Nature* **227**, 936 (1970).

[19] W.H. Press, *Astrophys. J.* **170**, L105 (1971).

[20] M. Davis, R. Ruffini, W.H. Press, and R.H. Price, *Phys. Rev. Lett.* **27**, 1466 (1971).

[21] S. Chandrasekhar and S.L. Detweiler, *Proc. Roy. Soc. Lond.* **A344**, 441 (1975).

[22] E.W. Leaver, *Proc. Roy. Soc. Lond.* **A402**, 285 (1985).

[23] E.W. Leaver, *Journal of Mathematical Physics* **27**, 1238 (1986), https://doi.org/10.1063/1.527130.

[24] E.W. Leaver, *Phys. Rev.* **D34**, 384 (1986).

[25] H.P. Nollert and B.G. Schmidt, *Phys. Rev. D* **45**, 2617 (1992).

[26] J.M. Maldacena, *Int. J. Theor. Phys.* **38**, 1113 (1999), [Adv. Theor. Math. Phys.2,231(1998)], arXiv:hep-th/9711200.

[27] F. Pretorius, *Phys. Rev. Lett.* **95**, 121101 (2005), arXiv:gr-qc/0507014.

[28] V. Cardoso, E. Franzin, and P. Pani, *Phys. Rev. Lett.* **116**, 171101 (2016), arXiv:1602.07309.

[29] V. Cardoso, S. Hopper, C.F.B. Macedo, C. Palenzuela, and P. Pani, *Phys. Rev. D* **94**, 084031 (2016).

[30] Quoting Subrahmanyan Chandrasekhar, "In my entire scientific life, extending over forty-five years, the most shattering experience has been the realization that an exact solution of Einstein's equations of general relativity provides the absolutely exact representation of untold numbers of black holes that populate the universe." S. Chandrasekhar, The Nora and Edward Ryerson lecture, Chicago April 22 1975.

[31] R. Brito, V. Cardoso, and P. Pani, *Lect. Notes Phys.* **906**, pp.1 (2015), arXiv:1501.06570.

[32] V. Cardoso and P. Pani, (2017), arXiv:1707.03021.

[33] V. Cardoso and P. Pani, *Nat. Astron.* **1**, 586 (2017), arXiv:1709.01525.

[34] C. Joachain, *Quantum collision theory* (North-Holland, 1975).

Appendix A

Generalized Frobenius approach to the Regge-Wheeler equation

Here we will generalize the Frobenius method [2], which is used to obtain solutions of linear, second-order and homogeneous ODEs. The Frobenius method consists of attempting a solution in the form of a series expansion about some point (usually at the origin). Insertion of this expansion into the ODE will turn it into an iteratively solvable recursion relation. The problem arises when there is divergent behaviour at the boundaries, in which case the solution is formally an asymptotic expansion. In this scenario we factor out the divergent behaviour, which usually contributes to simplify the recursion relation greatly.

A famous example of this method is the obtention of the Hydrogen atom energy spectrum from the Schrodinger equation: the centrifugal barrier factor $\sim r^{-l}$ is extracted and the result is a 2-term recursion relation [14]. Since the divergent behaviour at the origin is removed, the series resulting from the simplified recursion relation should converge. However, this only occurs for a specific combination of the constants involved, the energy quantization relation. The same method applies in the determination of the harmonic oscillator allowed energies.

Therefore, it is natural to expect that a similar Frobenius approach would yield the Schwarzschild black hole quasinormal modes, by requiring a truncation of the series. Unfortunately, there are a number of complications: First of all there is a causally disconnected region at $r < r_0 = 2M$, so an expansion at the origin is not possible. Secondly, by looking at the plot of the Regge-Wheeler potential 2.1 we see that there is no possiblity of bound states (hence the *quasinormal* behaviour). Third and most importantly, because of the previous point, the boundary behaviour is non-trivial and thus difficult to extract from the series expansion.

The idea here is to start with a generic expansion of the form

$$\psi(r) = g(r) \sum_{n=0}^{\infty} A_n (r - r_0)^n, \tag{A.1}$$

where $g(r)$ is the function responsible for capturing the boundary behaviour at r_0. What is novel in our approach is that we will keep $g(r)$ arbitrary until the recursion relation is obtained. Then, by requiring that the number of terms in the recursion relation for A_n is minimal, the explicit form of $g(r)$ becomes automatically determined.

For simplicity we choose $r_0 = 2M$, so we will expand around the horizon. In fact, $r \to r_0$ is a singular point [2] of the ODE (2.29) but since

$$\lim_{r\to r_0}(r-r_0)\frac{f'}{f} = 1 \tag{A.2}$$

and

$$\lim_{r\to r_0}\frac{(r-r_0)^2}{f^2}\Big(\omega^2 - f\Big(\frac{l(l+1)}{r^2} + f'\frac{1-s^2}{r}\Big)\Big) = r_0^2\omega^2 \tag{A.3}$$

are both finite, Fuchs' theorem ensures that the Frobenius method will result in a valid solution.

If we want to decouple $g(r)$ from the recursion relation it must satisfy

$$g'(r) = g(r)\sum_{j=0}^{\infty} a_j (r-r_0)^{j+z} \tag{A.4}$$

where $z \in \mathbb{Z}$ allows for negative powers of $(r - r_0)$, and the coefficients a_j will be such that the relation for A_n is the most simple.

Before expansion (A.1) is inserted into the Regge-Wheeler equation (2.29) it is best to compute its derivatives first:

$$\psi'(r) = g(r)\sum_{n}^{\infty}(r-r_0)^n\Big(A_{n+1}(n+1) + \sum_{j=0}^{\infty} a_j A_{n-j-z}\Big) \tag{A.5}$$

$$\psi''(r) = g(r)\sum_{n}^{\infty}(r-r_0)^n\Big(A_{n+2}(n+2)(n+1) + \sum_{j=0}^{\infty} a_j A_{n-j-z+1}(2(n+1)-j-z) + \sum_{j,j'=0}^{\infty} A_{n-j-j'-2z}a_j a_{j'}\Big) \tag{A.6}$$

Now we just have to insert the above into the Regge-Wheeler equation (2.29) and hope for suitable values of a_j to simplify the recursion relation. For $z < -1$ and $j > 2$ we get an higher number of recursion terms than before, thus the expansion (A.4) is only useful if we set $z = -1$ and $a_{j\geq 3} = 0$.

With these restrictions the following 5-term recursion relation is obtained.

$$\begin{aligned}
&A_n\big(r_0^4\omega^2 + r_0^2(n+a_0)^2\big)\\
&+ A_{n-1}\big(r_0(n-1-l(l+1)-\alpha+a_0) + 4r_0^3\omega^2 - r_0^2(2n-1)a_1 + 2r_0^2 a_1 a_0\big)\\
&+ A_{n-2}\big(r_0^2(6\omega^2 + a_1^2 + 2a_2(n-1+a_0)) - l(l+1) + (n-2)(n+2r_0-3) + a_1 r_0 + (2(n+r_0)-5)a_0 + a_0^2\big)\\
&+ A_{n-3}\big(4r_0\omega^2 + 2r_0^2 a_1 a_2 + 2a_0 a_1 + r_0 a_2 + (2(n+r_0)-6)a_1\big)\\
&+ A_{n-4}\big(r_0^2 a_2^2 + a_1^2 + \omega^2 + (2(n+r_0)-7)a_2 + 2a_0 a_2\big) = 0
\end{aligned} \tag{A.7}$$

with $n \geq 0$ and $A_{n<0} = 0$.

The indicial equation ($n = 0$) reads

$$A_0\big(r_0^4\omega^2 + r_0^2(n+a_0)^2\big) = 0, \tag{A.8}$$

which for non-vanishing A_0 implies that $a_0 = \pm i\omega r_0$.

Now we want to determine a_1 and a_2 such that the A_{n-4} factor, $(r_0^2 a_2^2 + a_1^2 + \omega^2 + (2(n+r_0)-7)a_2 + 2a_0 a_2$, vanishes. Notice that a_2 must be zero since it is the only coefficient multiplying n. Finally, with a_2 zero we have that $a_1^2 + \omega^2$ must vanish, which fixes $a_1 = \pm i\omega$.

Therefore, the recursion relation reduces to

$$\begin{aligned}
&A_n\big(r_0^2 n(n-2ir_0\omega)\big) \\
&+ A_{n-1}\big(r_0(-l(l+1)+2(n-1)^2+(n-1)(-1-6ir_0\omega)-\alpha)\big) \\
&+ A_{n-2}\big((l(l+1)+(n-2)(1-(n-2)+6ir_0\omega))\big) \\
&+ A_{n-3}\big(2i\omega(n-3)\big) = 0,
\end{aligned} \tag{A.9}$$

the already known recursion relation for the expansion around r_0 when the behaviour at $r \to r_0$ is extracted.

Indeed, if we choose the minus signs in both a_0 and a_1 we get

$$g'(r) = g(r)\Big(\frac{a_0}{r-r_0} + a_1 + a_2(r-r_0)\Big) = -ig(r)\omega\Big(\frac{r_0}{r-r_0}+1\Big) \tag{A.10}$$

which integrated gives

$$g(r) \propto e^{-i\omega\big(r + r_0\log(r-r_0)\big)} \tag{A.11}$$

the *ingoing* boundary condition at the horizon (2.34).

For curiosity sake, to eliminate the factor of A_{n-3} in (A.7) one needs $a_1 = 0$ and $a_2 = -4\omega^2$, in which case $g(r) = e^{-2\omega^2(r-r_0)^2}(r-r_0)^{-i\omega}$, a Gaussian behaviour centered at r_0 with deviation $\propto \frac{1}{\omega}$ (higher frequency corresponding to better localized wavepacket at r_0).

Importantly, we cannot eliminate the factors of A_n and A_{n-2} in (A.7) since there is an n^2 dependence and the a_j coefficients only have factors of n at most (because (2.29) is a *linear* 2nd order differential equation). The same happens with A_{n-1}, since fixing a_1 will cancel out a_0 in the same factor of A_{n-1} in Eq. (A.7), and vice-versa.

In reality, albeit not a rigorous statement, it seems that for every point one chooses to expand around there are always three terms in the 5-term recursion relation which are impossible (by the method presented) to make disappear. In fact, the most simplified recursion relation obtained so far is the 3-term recursion relation first obtained by Leaver [22], for which all factors have unsurprinsingly an n^2 dependence.

Despite all the previous reasoning, there is no real practical need for a closed expression for the quasinormal frequencies since nowadays these values can be determined to (virtually) arbitrary precision through the use of numerical methods [15].

Appendix B

Quasinormal modes

B.1 Sturm-Liouville theory in open systems

Taking a time dependence $\Psi(x,t) = e^{-i\omega t}\psi(x)$, the wave equation (1.6) can be put into the form

$$\mathcal{L}\psi = \omega^2\psi\,, \quad \mathcal{L} = -\frac{d^2}{dx^2} + V(x)\,. \tag{B.1}$$

This is an eigenvalue equation, where the set $\{\omega^2\}$ is determined by the solution $\psi(x)$ of this ODE, subject to the desired boundary conditions.

Open systems (i.e. with outgoing waves at the boundaries) are distinctively non-hermitian, so that, $\omega^2 \in \mathbb{C}$. One can see this explicitly by the following reasoning: take ψ_n and ψ_m to be solutions of Eq. (B.1) with some BC at $x = a$ and $x = b$. Integrating by parts yields

$$\int_a^b \psi_n^*\,\mathcal{L}\,\psi_m\,dx = \int_a^b (\mathcal{L}\psi_n)^*\psi_m\,dx - \left[\psi_n^*\psi_m' - (\psi_n*)'\psi_m\right]_a^b. \tag{B.2}$$

If ω_n and ω_m are the eigenvalues corresponding to ψ_n and ψ_m, respectively, the above simplfies to

$$\left((\omega_n^2)^* - \omega_m^2\right)\int_a^b \psi_n^*\,\psi_m\,dx = \left[\psi_n^*\psi_m' - (\psi_n^*)'\psi_m\right]_a^b. \tag{B.3}$$

Considering Dirichlet or Neumann boundary conditions at $x = a$ and $x = b$ makes the *rhs* of this equation vanish. Assuming that ψ_n and ψ_m are nondegenerate this would further imply that different eigenfunctions are orthogonal (and can be made to be orthonormal) and thus $\omega_n \in \mathbb{R}$ for any n. In these conditions the operator $\mathcal{L}$ is said to be *Hermitian*.

In an open system (with no external influence), one of the boundary conditions can be taken to be purely outgoing and the other to be some combination involving a reflection. For simplicity, let us take $\psi(x \to b) = e^{i\omega x}$ and $\psi(a) = 0$ (equivalent to the presence of a perfect mirror at $x = a$). Hence, we have in Eq. (B.3) that

$$\left((\omega_n^2)^* - \omega_m^2\right)\int_a^b \psi_n^*\,\psi_m\,dx = i(\omega_n^* + \omega_m)e^{i\Re[\omega_m-\omega_n]b}e^{-\Im[\omega_n+\omega_m]b} \tag{B.4}$$

which for $b \to \infty$ only converges to zero if $\Im[\omega_n + \omega_m] > 0$ for any n, m. If we take $n = m$ the above reduces to

$$-\Im[\omega_n^2] \int_a^b |\psi_n|^2 \, dx = \Re[\omega_n] e^{-2\Im[\omega_n]b}. \tag{B.5}$$

Noting that $\Im[\omega^2] = 2\Re[\omega]\Im[\omega]$ we can simplify this relation (in case $\Re[\omega_n] \neq 0$) to

$$\Im[\omega_n] = -\frac{1}{2} \left(\int_a^b e^{2\Im[\omega_n]b} \, |\psi_n|^2 \, dx \right)^{-1}. \tag{B.6}$$

This shows that $\Im[\omega_n] < 0$ for any n, due to the absolute positivity of the integral inside brackets. Thus, we can generally state that QNM frequencies have the form $\omega = \omega_R - i|\omega_I|$ which, for the assumed time dependence $\sim e^{-i\omega t}$, produces an exponential decay $\sim e^{-|\omega_I|t}$. This is a general fact of open systems with outgoing boundary conditions: $|\omega_I|$ contains the information about the dissipation of energy of the perturbation to the exterior. If we took $\sim e^{i\omega t}$ instead, we would naturally obtain $\Im[\omega_n] > 0$, and the perturbation would still exponentially decay in time.

The fact that $\Im[\omega_n] < 0$ also means that eigenfunctions are not orthogonal, through Eq. (B.4) ($\Im[\omega_n + \omega_m] < 0$), nor normalizable, through Eq. (B.5) due to the divergent quantity $\lim_{b\to\infty} e^{-2\Im[\omega_n]b} = \infty$.

It is also interesting to take the following intepretation of Eq. (B.6). The factor $e^{\Im[\omega_n]b}$ counters the diverging behaviour of ψ_n near $x \sim b$ so that $e^{2\Im[\omega_n]b} \, |\psi_n|^2$ is finite and can be interpreted as a probability amplitude (with no dimensions). If $V(x)$ is peaked at some $x = L + a$ then we expect our waves to be trapped between the mirror and the peak of the potential and the integral in (B.6) can be roughly approximated to $\int_a^{L+a} 1 \, dx$ so that we get $\Im[\omega] \sim -1/2L$, the inverse time that a wave takes to go back and forth in the space where it is (partially) confined and also importantly, the time difference between consecutive *echoes*.

For completeness we note that in case both boundaries are open ($\psi(x \to a) = e^{-i\omega x}$) instead of Eq. (B.6) we get

$$\Im[\omega_n] = -\frac{1}{2} \left(\int_a^b \left(e^{2\Im[\omega_n]b} + e^{-2\Im[\omega_n]a}\right) |\psi_n|^2 \, dx \right)^{-1} \tag{B.7}$$

and the previous argument tells us that if our potential has two peaks distanced by L then $\Im[\omega] \sim -1/L$, which is double the value of the previous case and can be explained due to trapped waves now leaking through both sides.

There is an additional detail worth discussing. The above result is not valid for open but *bounded* systems. These are conservative systems that have a BC of the form $\sim e^{-|E|x}$ at infinity, which are included in our description if $\omega = i|E|$ where $\{E_n\}$ corresponds to the energy eigenvalues. Physical examples include the Schrödinger or Klein-Gordon equations with a Coulomb potential (the Hyrdogen atom model). Since now $\Im[\omega_n] > 0$, Equations (B.6) and (B.7) cannot be true. However, since $E_n \in \mathbb{R}$ then in this case $\Re[\omega_n] = 0$ and the step from (B.5) to (B.6) is not true, i.e. both sides of Equation (B.5) are identically zero. Thus, it should be added that equations (B.6) and (B.7) only describe open and *unbounded* systems, where *dissipation* is present.

B.2 Dirac delta spectrum

Here we compute the QNMs for a system composed of: a single Dirac delta potential, a single delta and a mirror, and two Dirac deltas separated by some distance.

B.2.1 Single Dirac delta

The Dirac delta potential is given by

$$V(x) = V_0\,\delta(x) \tag{B.8}$$

with $V_0 > 0$.

If we take the regions $I =]-\infty, 0[$ and $II =]0, +\infty[$ then $\psi_I(x) = e^{-i\omega x}$ and $\psi_{II}(x) = e^{i\omega x}$ to agree with the outgoing boundary conditions and the continuity requirement $\psi_I(0) = \psi_{II}(0)$. The condition for QNMs comes from integrating wave equation (B.1) with potential (B.8) in a vanishing neighbourhood of $x = 0$,

$$\psi'_{II}(0) - \psi'_I(0) - V_0\psi(0) = 0 \tag{B.9}$$

which yields the single mode

$$\omega = -i\frac{V_0}{2}\,, \tag{B.10}$$

a purely imaginary QNM.

B.2.2 Delta & mirror

Here we use the same potential but supplied with a Dirichlet boundary condition at $x = -L$ (corresponding to a perfect mirror). The regions of interest are $I =]-L, 0[$ and $II =]0, +\infty[$ with $\psi_I(x) = e^{-i\omega x} + Ae^{i\omega x}$ and $\psi_{II}(x) = Be^{i\omega x}$, the latter already takes into account the outgoing BC at infinity.

Continuity at $x = 0$ yields $B = 1 + A$. The mirror condition $\psi_I(-L) = 0$ implies $A = -e^{i\omega 2L}$ so that

$$\psi_I(x) = e^{-i\omega x} - e^{i\omega(x+2L)}\,, \tag{B.11}$$

the first term in the rhs is travelling in the direction of the mirror where the second is the reflected wave, notice the $-$ sign (the reflectivity of a mirror) and how the incident wave is delayed by $2L$ from the reflected one, this is the rough distance observed between *echoes* in a scattering experiment.

Condition (B.9) now yields

$$e^{i\omega 2L}(-1)R_\delta(\omega) = 1 \tag{B.12}$$

with

$$R_\delta(\omega) = \frac{V_0}{2i\omega - V_0} \tag{B.13}$$

the reflectivity of a single Dirac delta potential, which diverges at the QNM (B.10).

If a plane wave is inserted between the mirror and the delta after a round trip it'll pick up a phase of $e^{i\omega 2L}$, a factor of $-1 = e^{i\pi}$ due to reflection at the mirror and an additional factor of $R_\delta(\omega)$ due to partial reflection at the delta. The total factor is exactly the *lhs* of Eq. (B.12), which implicitly yields the QNMs by equating it to unity. It should also be noted that in the limit $V_0 \to \infty$ the delta acts like a perfect mirror, since $R_\delta(\omega) \to -1$, thus turning Eq. (B.12) into $e^{i\omega 2L} = 1$, the well-known relation for the normal modes of a string of length L.

Unfortunately, Eq. (B.12) is a trascendental equation and thus cannot be solved explicitly. Nevertheless, it can be solved iteratively through the following procedure. If $\omega = \omega_R + i\omega_I$ then Eq. (B.12) can be written in system form,

$$\omega_R 2L + \pi + \arg R_\delta(\omega) = 2n\pi \tag{B.14}$$

$$-\omega_I 2L + \log |R_\delta(\omega)| = 0, \tag{B.15}$$

which can be solved in a convergent procedure by first computing R_δ for $\omega_{(i)}$ and using the above system to get $\omega_{(i+1)}$:

$$\omega_{(i+1)} = \frac{n\pi}{L} + \frac{1}{2L} \arg\left(1 - i\frac{2\omega_{(i)}}{V_0}\right) - \frac{i}{2L} \log\left|1 - i\frac{2\omega_{(i)}}{V_0}\right|. \tag{B.16}$$

Taking the *ansatz* $\omega_{(0)} = 0$ we get at first order $\omega_{(1)} = \frac{n\pi}{L}$, the string normal modes. Quasinormal behaviour is only obtained at second order, where

$$\omega_{(2)} = \frac{n\pi}{L} - \frac{1}{2L} \arctan\frac{2n\pi}{LV_0} - \frac{i}{4L} \log\left(1 + \frac{4n^2\pi^2}{L^2V_0^2}\right), \tag{B.17}$$

which, in the limit $n \gg 1$, simplfies to

$$\omega_{(2)} \approx \frac{n\pi}{L} - \frac{i}{2L} \log\frac{2n\pi}{LV_0}\,, \tag{B.18}$$

whereas in the opposite limit ($LV_0 \gg 1$) it reduces to

$$\omega_{(2)} \approx \frac{n\pi}{L}\left(1 - \frac{1}{LV_0}\right) - i\frac{n^2\pi^2}{L^3V_0^2}\,. \tag{B.19}$$

Notice how the potential strength V_0 has little influence on the real part but a considerable one on the imaginary part. It is expected that for larger L or V_0, the waves trapped inside region I last longer, corresponding to a smaller $|\omega_I|$, in agreement with all the above expressions for $\omega_{(2)}$.

B.2.3 Two deltas

Another way to construct a lossy cavity is with two deltas separated by a distance L,

$$V(x) = V_0\big(\delta(x) + \delta(x + L)\big). \tag{B.20}$$

It is straightforward to show that the condition for QNMs is given by

$$e^{i\omega 2L} R_\delta^2(\omega) = 1. \tag{B.21}$$

Notice the similarities with Eq. (B.12) where the reflectivity of the mirror (-1) gets replaced by the reflectivity R_δ of the additional delta. Following the previous subsection we can solve the above iteratively through the prescription

$$\omega_{(i+1)} = \frac{n\pi}{L} + \frac{1}{L}\arg\left(1 - i\frac{2\omega_{(i)}}{V_0}\right) - \frac{i}{L}\log\left|1 - i\frac{2\omega_{(i)}}{V_0}\right| \tag{B.22}$$

which, using the *ansatz* $\omega_{(0)} = 0$, yields again $\omega_{(1)} = \frac{n\pi}{L}$ and

$$\omega_{(2)} = \frac{n\pi}{L} - \frac{1}{L}\arctan\frac{2n\pi}{LV_0} - \frac{i}{2L}\log\left(1 + \frac{4n^2\pi^2}{L^2V_0^2}\right). \tag{B.23}$$

Note the similarities with Eq. (B.17). More specifically the relation

$$\Im[\omega_{(2)}]_{\,\text{(two deltas)}} = 2\Im[\omega_{(2)}]_{\,\text{(delta \& mirror)}}, \tag{B.24}$$

which confirms the interpretation given in the last paragraphs of Section B.1.

For completeness, we present the limiting cases $n \gg 1$ and $LV_0 \gg 1$ which are respectively given by

$$\omega_{(2)} \approx \frac{n\pi}{L} - \frac{i}{L}\log\frac{2n\pi}{LV_0}, \tag{B.25}$$

and

$$\omega_{(2)} \approx \frac{n\pi}{L}\left(1 - \frac{2}{LV_0}\right) - i\frac{2n^2\pi^2}{L^3V_0^2}. \tag{B.26}$$

B.3 Rectangular barrier spectrum

Here we will ompute the QNMs of a single rectangular barrier potential, and of a lossy cavity composed by a barrier and a perfect mirror.

B.3.1 Single barrier

The barrier potential is taken as

$$V(x) = \begin{cases} 0 & \text{if } x \in]-\infty, 0[\,\cup\,]a, \infty[\\ V_0 & \text{if } x \in [0, a] \end{cases}. \tag{B.27}$$

If we call the regions $I =]–\infty, 0[$, $II = [0, a]$ and $III =]a, \infty[$, Eq. (B.1) is trivially solved for all regions by imposing smoothness of ψ at $x = 0$ and $x = a$. From the outgoing BC we have that $\psi_{III}(x) = e^{i\omega x}$. In region II we obtain $\psi_{II}(x) = Ae^{i\Omega x} + Be^{-i\Omega x}$ (with $\Omega = \sqrt{w^2 - V_0}$), which by requiring smoothness at $x = a$ leads to

$$A = \frac{1}{2}e^{ia(\omega-\Omega)}\left(1 + \frac{\omega}{\Omega}\right), \quad B = \frac{1}{2}e^{ia(\omega+\Omega)}\left(1 - \frac{\omega}{\Omega}\right) \tag{B.28}$$

In region I, from the outgoing BC, we simply have $\psi_I(x) = e^{-i\omega x}$. Now finally, requiring smoothness at $x = 0$ yields the condition for the QNMs:

$$e^{2i\Omega a} = \frac{(\Omega + \omega)^2}{(\Omega - \omega)^2}, \tag{B.29}$$

which can be written as

$$e^{2i\Omega a} R_s^2(\omega) = 1 \tag{B.30}$$

with

$$R_s(\omega) = \frac{(\Omega - \omega)}{(\Omega + \omega)} \tag{B.31}$$

the *reflectivity* of the Heaviside step function potential $V_s(x; 0) = V_0\,\Theta(x)$.

The square barrier potential is the intersection of two step functions, $V(x) = V_s(x; 0)\,V_s(-x; a)$. If we take ω to be purely real, a wave that makes a round trip in the barrier picks up the factor in the *lhs* of Eq. (B.30): it is partially reflected (being attenuated by R_s) at each end of the barrier and obtains a phase corresponding to the distance travelled (twice the barrier length a), $e^{i\Omega 2a}$.

Now, as we did before for the delta potential, we can solve Eq. (B.30) iteratively through

$$\Omega_{(i+1)} = \sqrt{\omega_{(i+1)}^2 - V_0} = \frac{n\pi}{a} - \frac{1}{a}\arg R_s(\omega_{(i)}) + i\frac{1}{a}\log|R_s(\omega_{(i)})|. \tag{B.32}$$

If we now take the *ansatz* $\Omega_{(0)} = 0$ meaning $\omega_{(0)} = \pm\sqrt{V_0}$ then $R_s(\omega_{(0)}) = -1$ (i.e. purely reflective wall) and the above gives $\omega_{(1)} = \pm\sqrt{\left(\frac{n\pi}{a}\right)^2 + V_0}$, the normal modes of a length a string at a "height" V_0. So at second order we get

$$\Omega_{(2)} = \frac{n\pi}{a} - \frac{i}{a}\log\frac{\sqrt{\left(\frac{n\pi}{a}\right)^2 + V_0} + \left|\frac{n\pi}{a}\right|}{\sqrt{\left(\frac{n\pi}{a}\right)^2 + V_0} - \left|\frac{n\pi}{a}\right|}, \tag{B.33}$$

or, equivalently

$$\omega_{(2)} = \sqrt{A - iB} = \pm\sqrt{\frac{\sqrt{A^2 + B^2} + A}{2}} - i\sqrt{\frac{\sqrt{A^2 + B^2} - A}{2}} \tag{B.34}$$

with

$$A = \left(\frac{n\pi}{a}\right)^2 + V_0 - \frac{1}{a^2}\log^2\frac{\sqrt{\left(\frac{n\pi}{a}\right)^2 + V_0} + \left|\frac{n\pi}{a}\right|}{\sqrt{\left(\frac{n\pi}{a}\right)^2 + V_0} - \left|\frac{n\pi}{a}\right|} \tag{B.35}$$

$$B = \frac{2}{a}\left|\frac{n\pi}{a}\right|\log\frac{\sqrt{\left(\frac{n\pi}{a}\right)^2 + V_0} + \left|\frac{n\pi}{a}\right|}{\sqrt{\left(\frac{n\pi}{a}\right)^2 + V_0} - \left|\frac{n\pi}{a}\right|}. \tag{B.36}$$

Furthermore, under the assumption of $A \gg B$ (not valid for the first few modes) Eq. (B.34) reduces to

$$\omega_{(2)} \approx \pm\sqrt{\left(\frac{n\pi}{a}\right)^2 + V_0} - \frac{i}{a}\frac{\left|\frac{n\pi}{a}\right|}{\sqrt{\left(\frac{n\pi}{a}\right)^2 + V_0}}\log\frac{\sqrt{\left(\frac{n\pi}{a}\right)^2 + V_0} + \left|\frac{n\pi}{a}\right|}{\sqrt{\left(\frac{n\pi}{a}\right)^2 + V_0} - \left|\frac{n\pi}{a}\right|}, \tag{B.37}$$

which, for $n \gg 1$, further simplifies to

$$\omega_{(2)} \approx \frac{n\pi}{a} - \frac{i}{a} \log \frac{4n^2\pi^2}{V_0 a^2}. \tag{B.38}$$

Fig. B.1 is a plot of the quasinormal frequencies ω, by numerically solving Eq. (B.30), for different values of $V_0 a^2$. The logarithmic dependence of ω_I both on $\tilde{V}_0$ and n in Eq. (B.38) is evident below.

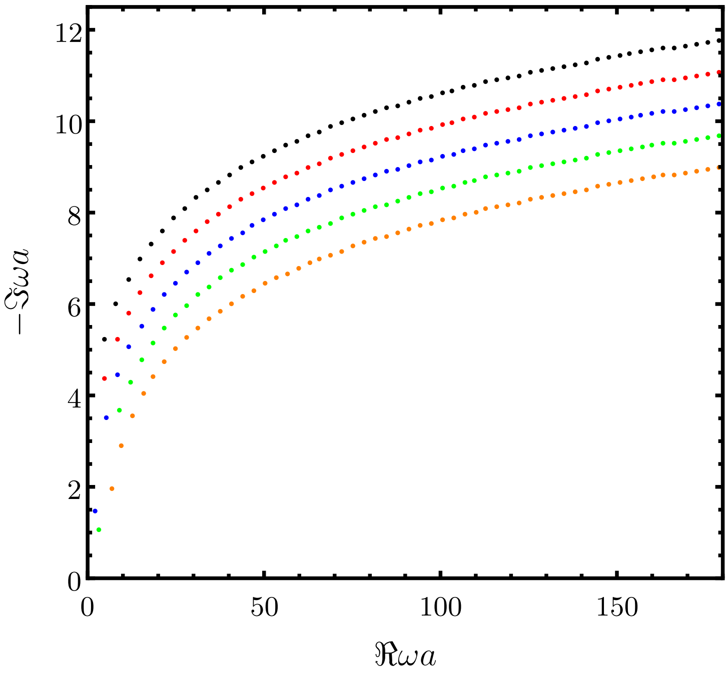

Figure B.1: QNM frequencies for the free case for different values of $V_0 a^2 = 1, 2, 4, 8, 16$ from top (black) to bottom (orange), respectively.

B.3.2 Barrier & mirror

When additional structure is included in region I the solution has to have the form $\psi_I(x) = e^{-i\omega x} + Ce^{i\omega x}$. Requiring $\psi_I(-L) = 0$ (perfect mirror) yields $C = -e^{2i\omega L}$. Then, imposing smoothness at $x = 0$, yields the QNM relation

$$e^{2i\Omega a} = \frac{(\Omega + \omega)^2 + V_0\, e^{i\omega 2L}}{(\Omega - \omega)^2 + V_0\, e^{i\omega 2L}}, \tag{B.39}$$

which allows direct comparison with Eq. (B.29). However, this is not the most suitable form to iteratively compute the mirror QNMs since it gives special attention to a whereas we have a new, more relevant length scale in the problem: L. With this in mind we can rearrange Eq. (B.39) into

$$e^{2i\omega L}(-1)R_b(\omega) = 1 \tag{B.40}$$

where

$$R_b(\omega) = \frac{(\omega^2 - \Omega^2)\sin\Omega a}{(\omega^2 + \Omega^2)\sin\Omega a + 2i\Omega\omega\cos\Omega a} \tag{B.41}$$

is the *reflectivity* of the square barrier potential $V(x)$ and (-1) is nothing but the reflectivity of the mirror (which must be unitary since it is perfectly reflecting). The factor $e^{i\omega 2L}$ accounts for the phase attained in a round trip between the mirror and the barrier.

Eq. (B.40) is in the same form of Eq. (B.30) and the physical interpretation is the same: a lossy optical resonator. Despite this, they are algebraically completely distinct due to the different expressions of $R_s(\omega)$ and $R_b(\omega)$ and hence we should expect both sets of QNMs also to differ considerably, even though physically both systems are just distinguished by some mirror placed at a distance L from the barrier.

The modes can be obtained through the iterative prescription:

$$\omega_{(i+1)} = \frac{n\pi}{L} - \frac{1}{2L}\arg\big(-R_b(\omega_{(i)})\big) + i\frac{1}{2L}\log|R_b(\omega_{(i)})|, \tag{B.42}$$

which, with the *ansatz* $\omega_{(0)} = 0$, leads to

$$\omega_{(2)} = \frac{n\pi}{L} - \frac{1}{2L}\left(\pi + \alpha(n) - \arctan\left(\frac{2\Omega_{(1)}\omega_{(1)}}{\Omega_{(1)}^2 + \omega_{(1)}^2}\cot\Omega_{(1)}a\right)\right) - \frac{i}{4L}\log\left(1 + \frac{4\,\omega_{(1)}^2\Omega_{(1)}^2}{V_0^2\,\sin^2\Omega_{(1)}a}\right), \tag{B.43}$$

that for $n \gg 1$ can be drastically simplified to

$$\omega_{(2)} \approx \frac{n\pi}{L} - \frac{i}{2L}\log\left(\frac{2n^2\pi^2}{V_0L^2|\sin(n\pi a/L)|}\right) \tag{B.44}$$

Note the similarities with Eq. (B.38). Both have the same structure apart for an exchange $a \leftrightarrow L$ and the $\sin(n\pi a/L)$ factor encorporating the spatial extent of the barrier into the mirror case QNMs.

The difference is that, for large V_0, we intuitively expect the first few modes to be very long lived due to having a ”frequency” lower than the barrier height. However, this is not apparent in Eq. (B.44). In this limit $\Omega_{(1)} \approx i\sqrt{V_0}$. If we also use $\sin ix = i\sinh x$ and $\log(1+x) \approx x$ for small x then Eq. (B.43) reduces to

$$\omega_{(2)} \approx \frac{n\pi}{L}\Big(1 - \frac{1}{\sqrt{V_0}L}\Big) - i\frac{4n^2\pi^2}{V_0L^3}e^{-2\sqrt{V_0}a} \tag{B.45}$$

corresponding to the modes sitting on the real axis in figures B.3 and B.4. The transition from this ”normal” behaviour to the usual QNM behaviour occurs when $\Omega_{(1)}$ goes from *imaginary* to *real*, which happens at

$$n \sim \bar{n} = \frac{\sqrt{V_0}L}{\pi} \tag{B.46}$$

and becomes naturally more evident for large V_0, when the cavity supports more long-lived modes.

Since we have 2 parameters (V_0a^2, L/a) we have to make a variety of plots to see the behavior of the modes. Numerical solution of (B.40) for different heights of the barrier yields Fig. B.2. We see that the general effect of having a reflecting wall at one side of the barrier is to lower $|\Im\omega|$ (compare with Fig. B.1).

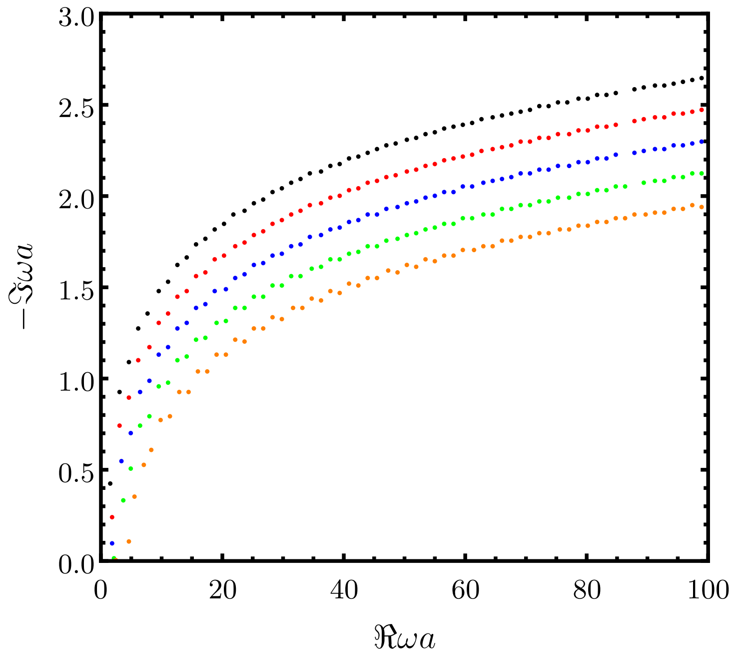

Figure B.2: QNM frequencies for the mirror case with $L = a$ for different values of $V_0a^2 = 1, 2, 4, 8, 16$ from top (black) to bottom (orange), respectively.

To see the QNMs for different cavity sizes we point out to Fig. B.3, which is in terms of L/a. Note the 'phase transition' between the contained 'normal' modes sitting on the real lines and the usual dissipative QNMs which can be seen more clearly in Fig. B.4.

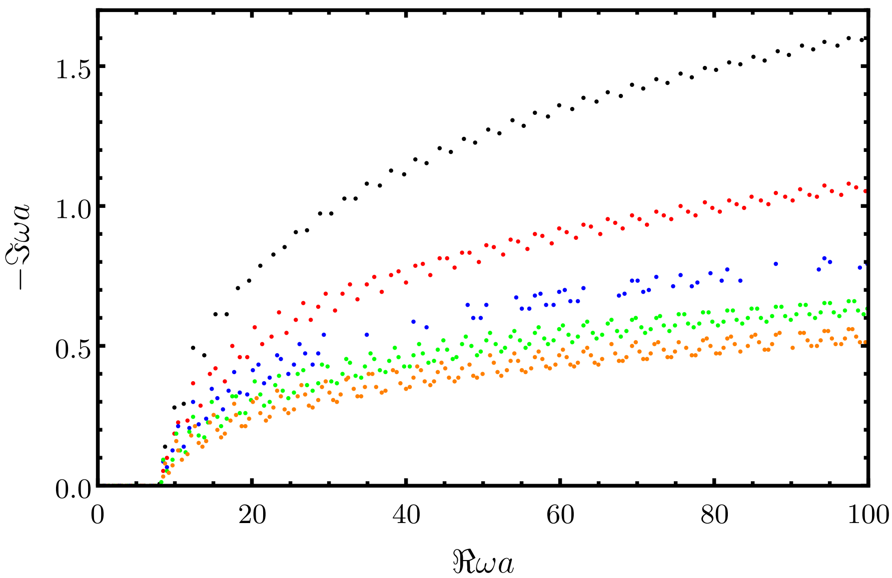

Figure B.3: QNM frequencies for the mirror case with $V_0a^2 = 64$ for different values of $L/a = 1, 2, 3, 4, 5$ from top (black) to bottom (orange), respectively.

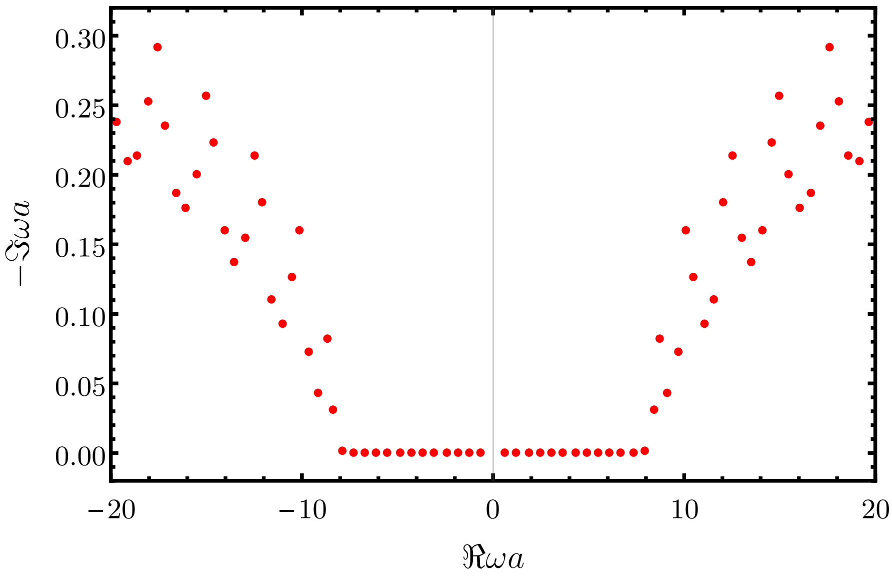

Figure B.4: Quasinormal transition for $V_0 a^2 = 64$ and $L = 2a$. The transition occurs for the mode $\bar{n} \approx 12.7324$ with $\Re\omega_{\bar{n}} a \approx \sqrt{V_0 a^2} = 8$.